Journal of Environmental Chemical Engineering 13 (2025) 116965

Contents lists available at ScienceDirect

Journal of Environmental Chemical Engineering

journal homepage: www.elsevier.com/locate/jece

Exploring bioactive compounds from rosemary waste for structural insights and food packaging innovation

Imane Ziani [a,b,*], Hamza Bouakline [a], Mohammed Merzouki [c], Marie-Laure Fauconnier [d], Farooq Sher [e,**], Nour Eddine Bentouhami [f], Abudukeremu Kadier [g,h], Sabah Ansar [i], Abdeslam Asehraou [f], Allal Challioui [c], Ali El Bachiri [a]

[a] Physical Chemistry of Natural Substances and Process Research Team, Laboratory of Applied Chemistry and Environment, Faculty of Sciences, Chemistry Department, Mohammed First University, Oujda, Morocco
[b] International Society of Engineering Science and Technology, Nottingham, United Kingdom
[c] Laboratory of Applied Chemistry and Environment, Faculty of Sciences, Chemistry Department, Mohammed First University, Oujda 60000, Morocco
[d] Laboratory of Chemistry of Natural Molecules, Gembloux Agro-Bio Tech, University of Liège, Liège, Belgium
[e] Department of Engineering, School of Science and Technology, Nottingham Trent University, Nottingham NG11 8NS, United Kingdom
[f] Laboratory of Bio-Resources, Biotechnology, Ethno-Pharmacology and Health., Faculty of Sciences, Mohammed First University, Oujda, Morocco
[g] Xinjiang Key Laboratory of Separation Material and Technology, The Xinjiang Technical Institute of Physics and Chemistry, Chinese Academy of Sciences, Urumqi 830011, China
[h] Center of Materials Science and Optoelectronics Engineering, University of Chinese Academy of Sciences, Beijing 100049, China
[i] Department of Clinical Laboratory Sciences, College of Applied Medical Sciences, King Saud University, P.O. Box 10219, Riyadh 11433, Saudi Arabia

ARTICLE INFO

Keywords:
Waste valorisation
Norursane-type triterpenoids
Solvent-based recrystallisation
Characterisation methods
Skin pigmentation
Molecular docking
Food packaging materials

ABSTRACT

This study presents a sustainable and innovative approach to waste valorisation by isolating and characterising bioactive norursane-type triterpenoids from the solid waste of *Rosmarinus tournefortii* de Noé. A cost-effective, solvent-based recrystallisation method was developed as an eco-friendly alternative to traditional chromatography techniques, which are often expensive and resource-intensive. Individual triterpenoids were structurally characterised using ATR-FTIR, CHNSO elemental analysis, 1D and ^{2}D NMR, UHPLC-MS/MS, and stereochemical analysis with Schrödinger's Maestro software. Their bioactivities were extensively evaluated. Notably, compound 3' exhibited enhanced antimicrobial activity in its amorphous form compared to its crystalline counterpart, highlighting the influence of physical structure on bioactivity. In contrast, the crystalline form of the same compound showed enhanced tyrosinase inhibitory activity, indicating that different physical states may favour different biological functions. Furthermore, the isolated compounds also demonstrated significant skin depigmentation properties through tyrosinase inhibition, with compound 2 showing the most potent effect. Molecular docking supported this activity, revealing a higher binding affinity than kojic acid. Compound 1 showed promising antidiabetic potential by outperforming acarbose in docking studies with α-amylase and α-glucosidase. These findings highlight the potential of norursane triterpenoids as multifunctional bioactive agents. It is hypothesised that such compounds, derived from agro-industrial waste, hold significant promise for use in advanced food materials. The study proposes their integration into porous food packaging systems for controlled release and targeted bioactivity, with attention to their interactions within food matrices.

1. Introduction

Global waste is expected to increase by 70 % to 3.4 billion tonnes annually by 2050 [1], with agricultural waste alone accounting for more than 2.8 billion tonnes per year [2]. Burning rice straw, among other negligence, is responsible for millions of tonnes of CO_2 and particulates released into the environment, exacerbating climate change. In response, renewable technologies such as valorisation and circular

* Corresponding author at: Physical Chemistry of Natural Substances and Process Research Team, Laboratory of Applied Chemistry and Environment, Faculty of Sciences, Chemistry Department, Mohammed First University, Oujda, Morocco.
** Corresponding author.
E-mail addresses: imane.ziani95@outlook.com (I. Ziani), Farooq.Sher@ntu.ac.uk (F. Sher).

https://doi.org/10.1016/j.jece.2025.116965
Received 11 February 2025; Received in revised form 20 April 2025; Accepted 6 May 2025
Available online 7 May 2025

bioeconomy uses are becoming increasingly popular [3], turning food and agri-food industry waste into valuable compounds to be used for medicines, food preservation, and material science [4]. These technologies reduce waste, lower carbon footprints, and offer natural alternatives to chemical additives, cutting down food industry waste by up to 50 % [5]. One promising area of valorisation lies in triterpenoids, particularly ursane-type triterpenoids, a subgroup of pentacyclic compounds known for their anti-inflammatory, anticancer, and antimicrobial properties [6].

Numerous studies have explored the isolation protocols for ursolic acid, a well-known ursane-type triterpenoid, from agricultural and food waste. For example, Frighetto et al. [7] isolated ursolic acid from apple peels by extraction with ethanol after removal of the n-hexane wax and then purified it by high-speed counter-current chromatography, while Cargnin et al. [8] subjected the dried apple pomace to treatment with refluxing ethanol, followed by chromatography on silica gel and recrystallisation in acetonitrile. Wang et al. [9] used counter-current chromatography with pH zone refinement, trifluoroacetic acid and ammonia to isolate ursolic and oleanolic acids. Although effective, these methods pose environmental and scalability problems due to the use of strong acids and organic solvents. The biological potential of these compounds is considerable. For instance, trans-OCMA from *Ligustrum lucidum* inhibits γ-secretase, reducing Aβ40 and Aβ42 levels with IC_{50} values of 1.17 and 0.30 μM, respectively, while also improving synaptic plasticity in APP/PS1 mice [10]. Similarly, (2α,19α)-2,19-dihydroxy-3-oxo-urs-12-en-28-oic acid from *S. mexicanum* exhibits tyrosinase inhibition (IC50 =8.03 μM) and melanin production suppression (IC50 =8.53 μM) [11]. Other triterpenoids, such as tormentic acid and arjunolic acid from *Myrianthus arboreus*, have demonstrated the capability to lower blood glucose levels and enhance lipid profiles in diabetic rats [12]. These examples highlight the need for greener, scalable methods to harness triterpenoids for therapeutic and environmental applications.

In contrast to the well-studied ursane-type triterpenoids, nor-ursane-type triterpenoids remain underexplored. Despite their distinct structural features and promising bioactivities, these compounds have received limited attention. Existing studies have employed solvent extraction, partitioning, and chromatographic purification to isolate them. For example, norursane-type compounds have been isolated from *Gelsemium elegans* [13] via methanol and acid-base fractionation and from *Dipsacus asper* using ethanol extraction, solvent partitioning, macroporous resin, and HPLC. Additional sources include *Syzygium szemaoense* [14], *Rumex japonicus* [15], and *Pterocephalus hookeri* [16], each requiring multi-step extraction and purification protocols. These methods, though effective, underscore the need for more sustainable and scalable alternatives.

In this context, rosemary, a widely recognised medicinal herb, offers a promising yet underutilised source of bioactive compounds, particularly pentacyclic triterpenoids [17]. Ursane-type triterpenoids were successfully obtained from its aerial parts by ethanol sonication and silica gel chromatography. Norursane-type triterpenoids have been obtained using comparable methods. For example, Zhong et al. [18] isolated three of these compounds using ethanol-assisted aqueous sonication, followed by silica gel chromatography and gradient elution based on methanol-chloroform mixtures. Similarly, Zhou et al. [19] used the same technique to isolate norursane-type triterpenoids from dry leaves and twigs, using different ethanol concentrations and fractionation on silica gel and Sephadex LH-20. Altinier et al. [20] isolated micromeric acid from rosemary leaves using methanol extraction, acid-base partitioning and HPLC purification. However, the use of rosemary waste, as opposed to fresh plant material, is barely mentioned in the literature.

The novelty of this study lies in utilising rosemary solid waste as a source of nor-ursane-type triterpenoids through a sustainable solvent-based recrystallisation method. This approach eliminates reliance on chromatographic purification, significantly reducing hazardous solvent use and energy consumption, and aligns with circular bioeconomy principles. Previous studies on rosemary have primarily focused on fresh plant material. Only a few have explored solid waste as a bioactive resource. For instance, Chen et al. [21] isolated labdane and isopimarane diterpenoids using supercritical CO_2 and ethanol extraction, followed by chromatography. A previous study [22] demonstrated the potential of rosemary by-products (*R. tournefortii* de Noé) for triterpenoid recovery using methanolic extraction and flash chromatography purification. However, chromatography remains the dominant method for obtaining pure compounds in all reported cases.

In contrast, the current study successfully isolates three previously unidentified norursane-type triterpenoids from the solid waste of *R. tournefortii* de Noé using a solvent-based recrystallisation strategy. Structural elucidation of the triterpenoids was achieved through ATR-FTIR, CHNSO elemental analysis, 1D and ^{2}D NMR spectroscopy (HSQC, HMBC, COSY), UHPLC-MS/MS as well as chiral configuration modelling using Schrödinger's Maestro software. Additionally, in vitro evaluations of antimicrobial activity and anti-tyrosinase potential were conducted, complemented by molecular docking studies to assess their inhibitory effects on key enzymes involved in blood sugar regulation and melanin synthesis (α-amylase, α-glucosidase, and tyrosinase). The substantial bioactive potential of these newly identified triterpenoids underscores their applicability in developing innovative therapeutic agents and highlights their relevance for sustainable practices in the food industry. Furthermore, this research explores the potential application of these bioactive compounds in porous materials for food preservation, with their stability, release mechanisms, and efficacy being key aspects of future investigations.

2. Material and methods

2.1. Plant material, extraction and isolation

2.1.1. Plant material and post-distillation solid waste collection

Fresh leaves of *Rosmarinus tournefortii* de Noé wild species were obtained from the Megrez forest zone in eastern Morocco [23]. Leaves were shade-dried at ordinary temperature for ten days. Afterwards, about 100 kg of dried leaves were steam-distilled on a pilot scale for three hours to obtain the essential oil [24]. The process was conducted using steam from an independent boiler set at a pressure of 2–2.5 bars, generating steam at 100–104 °C. The steam passed through the plant material from bottom to top, ensuring efficient extraction. A two-wall cooling system, incorporating a chilled water compressor (0–4 °C) and tap water, ensured optimal condensation. Pressure gauges installed at the head of the still and at the outlet allowed precise monitoring and control of the pressure throughout the process (Fig. 1**(a)**). After distillation, the solid waste was separated from the water and left to dry for around 15 days.

2.1.2. Extraction and isolation of norursane triterpenoids

The dried solid waste was subjected to two different extraction methods (Fig. 1**(b)**). In the first method (A), the solid waste was directly extracted with 250 mL of methanol. Methanol was selected as the solvent due to its polarity and ability to dissolve a wide range of organic substances, particularly polar and semi-polar compounds such as pentacyclic triterpenoids [25]. In contrast, in the second method (B), extraction was carried out successively with 250 mL hexane followed by ethyl acetate, using a soxhlet apparatus for 8 hours in both cases. n-Hexane was initially used to dissolve non-polar lipophilic compounds, while ethyl acetate was subsequently employed to extract more polar compounds, including pentacyclic triterpenoids [26]. This sequential extraction efficiently isolated a broad spectrum of bioactive compounds, optimizing yield and purity.

The methanol solution (A) was immediately bleached with activated charcoal and filtered, producing a light-brown filtrate, which was then kept in the dark until a precipitate appeared. Activated charcoal

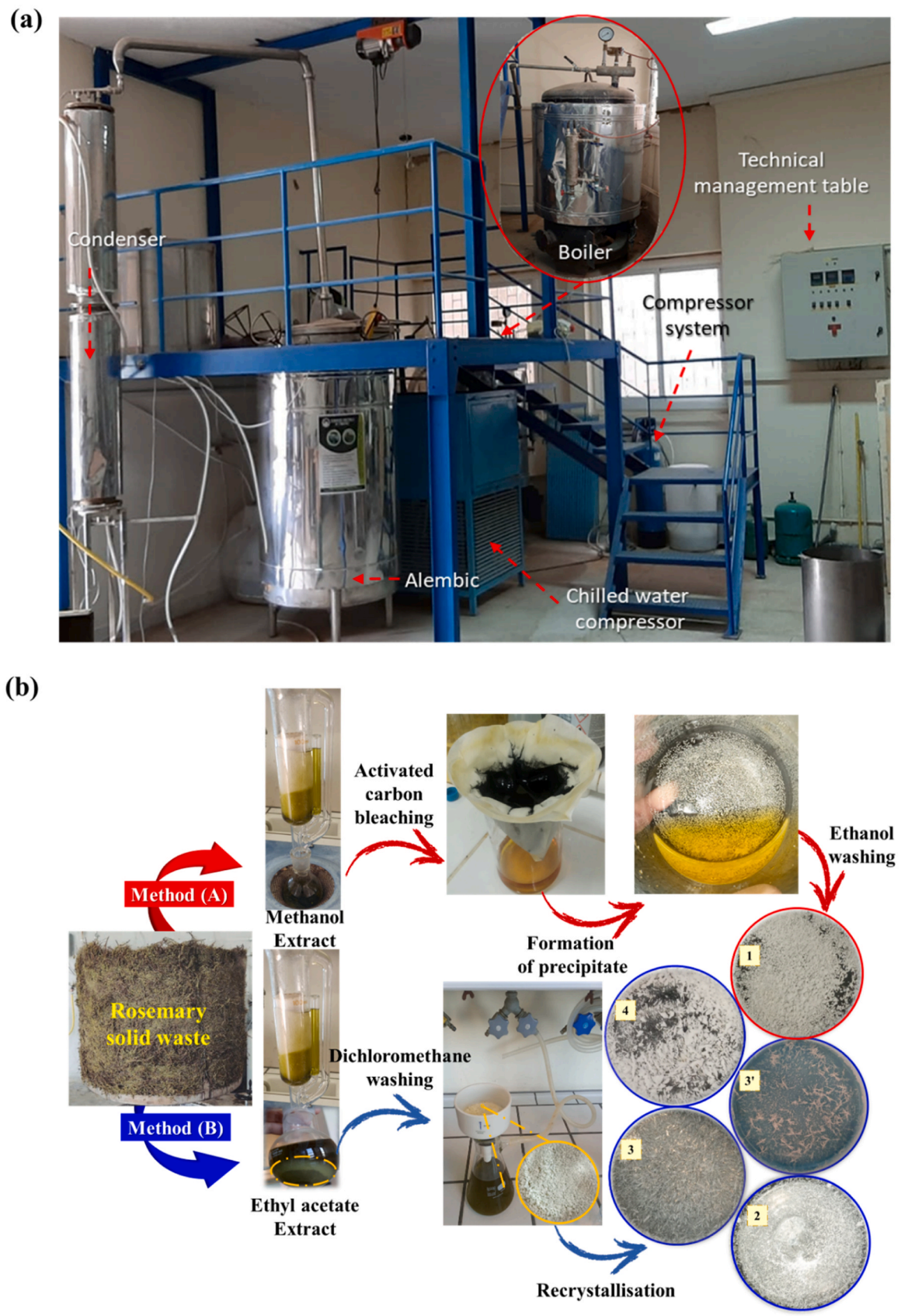

Fig. 1. (a) Pilot-scale steam distillation process and (b) Extraction and purification of *Rosmarinus tournefortii* de Noé solid waste.

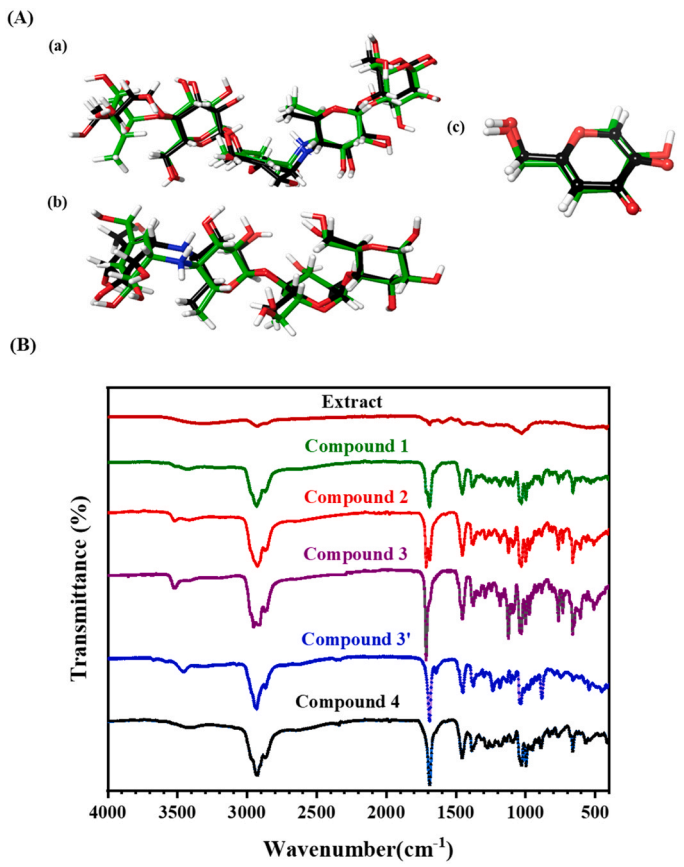

Fig. 2. (A) (a) Superposition of the re-docked conformation of the co-crystallized ligand Acarbose (black) with the experimental ligand of Alpha-Amylase (green), showing a calculated RMSD value of 1.258 Å. (b) Superposition of the re-docked conformation of the co-crystallized ligand Acarbose (black) with the experimental ligand of Alpha-Glucosidase (green), with a calculated RMSD value of 1.891 Å. (c) Superposition of the re-docked conformation of the co-crystallized ligand Kojic acid (black) with the experimental ligand of Tyrosinase (green), showing a calculated RMSD value of 0.964 Å. (B) ATR-FTIR of the isolated norursane-type triterpenoids from rosemary solid waste.

removes impurities such as pigments and stabilising substances. Eliminating these components alters the solubility equilibrium, leading to the precipitation of the purified compounds. The resulting precipitate was purified by washing several times with methanol, resulting in a pure white solid. Meanwhile, the ethyl acetate extract (B) was concentrated using a rotary evaporator and then washed three times with dichloromethane to remove chlorophylls. Four pure compounds were isolated from the washed ethyl acetate extract (B) by recrystallisation from ethanol, 75 % ethanol/methanol, 50 % ethanol/methanol and methanol. These recrystallisation conditions were selected based on the differing solubility profiles of the target compounds in various solvent systems, aiming to maximise purity while minimising material loss during purification.

2.2. Analytical instrumentation

The isolated compounds from rosemary by-products were analyzed using advanced analytical techniques. Attenuated total reflectance-Fourier transform infrared (ATR-FTIR) spectroscopy was performed using a Jasco 4700-FTIR spectrometer, covering wavelengths from 500 to 4000 cm^{-1} [27]. CHNSO elemental analysis was performed using an EA 3000 to determine the pure compounds' carbon, hydrogen, and oxygen composition. Nuclear magnetic resonance (NMR) spectroscopy, including one-dimensional (1D) and two-dimensional (2D) techniques, including heteronuclear single quantum coherence (HSQC), heteronuclear multiple bond correlation (HMBC) and homonuclear correlation spectroscopy (COSY), was performed using a Bruker Avance 700 MHz spectrometer [28]. Chemical shifts (δ) were recorded using tetramethylsilane (TMS) as an internal reference and calibrated against the residual proton solvent signals. For DMSO, the shifts were recorded at 2.50 ppm for ^{1}H and 39.5 ppm for HMBC and HSQC. In ethanol, the values were 1.06, 3.44 and 4.35 ppm for ^{1}H, and 18.51 and 56.07 ppm for HMBC and HSQC.

Similarly, the shifts appeared for methanol at 3.17 and 4.10 ppm for ^{1}H, with 48.59 ppm for HMBC and HSQC NMR [29]. Ultra-high performance liquid chromatography-tandem mass spectrometry (UHPLC-MS/MS) was performed utilising an Agilent 1290 Infinity II LC UHPLC in conjunction with an Agilent 6470 Triple Quad LC-MS/MS mass spectrometer. Mass spectra were evaluated with MassHunter ChemStation software across a scan range of 50–1100 *m/z* to determine the molecular weight and composition of the isolated compounds. Due to the specifications of this system, the mass spectrometry data are limited to two decimal places. To visualise the chiral carbons (*R* or *S*) configuration on Schrödinger's Maestro, molecules are first prepared using the LigPrep module to generate 3D conformations, such as stereoisomers [30]. After optimisation, Maestro's 3D visualisation capabilities are used to visualise the chiral carbons and their bonds with adjacent functional groups. Based on Cahn-Ingold-Prelog rules [31], the configuration can be viewed by looking at substituent priority. The users can highlight or annotate the configuration on the structure itself to ensure easy identification of chirality prior to molecular docking simulations.

2.3. Microbial growth suppression

The agar diffusion method described by Barros et al. [32] was applied to moderate the antimicrobial activity of compounds isolated from solid waste of rosemary against a range of pathogenic microbes. The tested strains consisted of two Gram-positive bacteria, namely *L. innocua* and *S. aureus*; two Gram-negative bacteria, which were *E. coli* and *P. aeruginosa*; along with two types of molds, *Geotrichum sp.* and *A. niger*; and finally, two yeast species, *Penicillium sp.* and *R. glutinis* [22]. The strains were modified and diluted to a density of 0.5 McFarland, corresponding to 10^{6} CFU/mL for bacteria and yeast and 10^{6} spores/mL for moulds [33]. The newly obtained cultures were subsequently applied onto the surfaces of Petri dishes, which had been earlier set up with Mueller-Hinton broth for bacteria and yeasts, along with sterile physiological water for moulds. In this method, 6 mm wells were created in the agar and inoculated with the bacteria or fungi intended for testing. The isolated compounds were placed into the wells at a concentration of 2 mg/mL, with a total volume of 10 µL per well. Following inoculation, the plates were initially incubated at 4 °C for 2 hours to allow for adequate diffusion of the compounds from the wells into the agar [34]. After this pre-incubation step, the plates were incubated at 30 °C for 24 hours for bacterial and yeast cultures to ensure proper growth conditions, while mold cultures were incubated at 25 °C for 24 hours. The antimicrobial effects of the isolated compounds were evaluated by measuring the size of the inhibition zones on the agar gel. *Gentamicin* and *cycloheximide* served as positive controls for bacteria and fungi, respectively.

2.4. Anti-melanogenic activity

The activity against tyrosinase of the isolated compounds was measured using mushroom tyrosinase enzyme, based on the method of Peng et al. [35], with a slight alteration. A range of sample concentrations (0.01, 0.05, 0.1, 0.2, 0.4, 0.6, 0.8, and 1 mg/mL) was prepared in appropriate solvents. For each assay, 0.01 mL of the test sample was mixed with 0.05 mL of mushroom tyrosinase solution (625 U/mL) and 0.25 mL of phosphate buffer (0.05 M, pH 6.5). Following a 15-minute

pre-incubation at 25 °C to stabilize the enzyme-substrate reaction, 0.4 mL of L-Dopa (1 mM) was added to start the enzyme-catalyzed reaction. The inhibitory activity of norursane-type triterpenoids was monitored by recording the absorbance at 475 nm every 15 seconds for 5 minutes, utilising a UV–VIS (Shimadzu UV 1650-PC) Spectrophotometer. The inhibitory kinetics were assessed by comparing the absorbance values of the isolated compounds to those of the negative control (which contained no test compound). The tyrosinase inhibition rate was calculated based on these measurements. Kojic acid was used as the reference standard.

2.5. Computer-based molecular docking

2.5.1. Ligand preparation

The ligands isolated from the solid waste of *R. tournefortii* de Noé required energy level adjustments. To achieve this, the LigPrep module in Maestro 13.8 (Schrodinger, LLC, New York, NY, USA) was used [36]. LigPrep converted 2D structures into optimised 3D conformations, applying energy minimization, assigning appropriate protonation states at physiological pH (~7), removing impurities or unwanted fragments, and generating relevant tautomeric forms and stereoisomers [37]. This step ensured that each molecular structure had the correct bond orders and was chemically accurate for docking. The inhibitors were then converted to SDF format and optimised using the default settings of the OPLS 2005 force field [38]. In this study, acarbose and kojic acid served as reference standards.

2.5.2. Protein structure preparation

For molecular docking investigations, the X-ray crystal structures of proteins were given by the Protein Data Bank. The structures included the "Structure of human pancreatic alpha-amylase in complex with the carbohydrate inhibitor acarbose" (PDB ID: 1B2Y) with clarity of 3.20 Å; the "Human lysosomal acid-alpha-glucosidase (GAA) crystal structure, complexed with acarbose" (PDB ID: 5NN8) with a resolution of 2.45 Å; and the "Crystal structure of tyrosinase from *Bacillus megaterium* in complex with the inhibitor kojic acid" (PDB ID: 3NQ1) with a resolution of 2.30 Å [39]. As PDB structures often lack information on connectivity, bond orders, and formal charges, protein structures were prepared by the Protein Preparation Wizard in Maestro [40]. This process included adding missing hydrogen atoms, assigning proper ionisation states, and energy minimisation. Only polar hydrogen atoms were displayed to simplify the analysis of the structures. To validate the docking procedure, the native co-crystallised ligand Acarbose was redocked into the catalytic pocket of Alpha-Amylase and Alpha-Glucosidase. In contrast, the native co-crystallised ligand Kojic acid was redocked into the catalytic pocket of Tyrosinase (**Fig. 2(A)**). The best conformations obtained were superimposed onto the crystallized structures to confirm alignment. The low RMSD values between the docked conformation and the native conformation (< 2 Å) further confirm the reliability of the docking protocol.

2.5.3. Grid-based ligand docking with energetic

The docking analysis was conducted using the Standard Precision (SP) mode of the Grid-based ligand docking with energetic (GLIDE) module within the Schrödinger suite, which balances computational efficiency and docking accuracy for evaluating ligand-receptor binding affinities. GLIDE uses a tiered filtering approach to position ligands within the protein's active site accurately [41]. The SP mode selects optimal ligand conformations based on scoring functions. Key steps in this workflow include preparing the protein structure, generating a receptor grid, processing ligand structures, and executing the docking procedure. The best-docked conformation was illustrated through 2D and 3D diagrams showing the interaction of the ligand with active site residues using BIOVIA Discovery Studio, 2021 [42].

2.6. Statistical analysis

Statistical analysis of the data was performed with SPSS software (Windows, version 20) by applying descriptive statistics, one-way ANOVA, and regression analysis. Variations between treatment groups were established by one-way analysis of variance and Tukey's HSD test for post hoc pair-wise comparisons at a significance level of 5 % ($p < 0.05$). Each experiment was repeated three times independently, and the results are expressed as mean values with respective standard deviations [22]. Statistical tests revealed significant differences among treatment groups; however, any groups with the same letter designation were not statistically different ($p \geq 0.05$).

3. Results and discussion

3.1. Structural characterisation techniques

3.1.1. Analysis of vibrational properties

FTIR spectroscopy represents the first analytical method used for studying the secondary structure of pentacyclic triterpenoids found in plants. This technique allows for analysing these compounds' specific vibrational frequencies and spectral characteristics, providing valuable information about their molecular structure and spatial arrangements [43]. The FTIR-ATR spectra of both the isolated compounds and the crude extract of rosemary solid by-products are illustrated in **Fig. 2(B)**. The IR spectra reveal prominent absorption bands in the high-wavelength region, specifically at 3450/3520 and 2920 cm^{-1}, corresponding to the asymmetric and symmetric stretching vibrations of the -OH and -CH_2 groups, respectively. Additionally, several significant bands in the fingerprint region were observed at 1690, 1450, 1390, 1250, 1050, 890, 750, and 650 cm^{-1}. Notably, the band at 1690 cm^{-1} is attributed to the stretching of the C═O bond in the -COOH functional group.

Furthermore, the bands at 1450 and 1390 cm^{-1} correspond to bending vibrations of the -OH, -CH_2, and CH_3 groups, along with skeletal bending vibrations. The bands at 1250 and 1050 cm^{-1} are associated with C-O stretching, among other vibrational modes. The strong absorptions at 890, 750, and 650 cm^{-1} specifically reflect the vibrations of the CH_2 group of alkenes. These findings align with previous research on functional groups in pentacyclic triterpenoids conducted by several researchers. For example, Yang et al. [44] reported similar attributions for O-H stretching vibrations at 3437 cm^{-1}, overlapping peaks of C-H stretching vibrations at 2935 cm^{-1}, and stretching vibrations of carbonyl groups at 1715 cm^{-1}. In another study, Kim et al. [45] isolated new ursane-type triterpenoid compounds and attributed characteristic absorption bands at 3378 cm^{-1} (hydroxyl), 1692 cm^{-1} (carbonyl), 1636 cm^{-1} (alkene), and 1056 cm^{-1} (methyl). Moreover, Fălămaş et al. [46], conducted research on betulin-like pentacyclic triterpenoids, revealing dominant IR absorption bands for OH, CH_3, CH_2, C═O, and C═C vibrations in the high-frequency region.

While these results confirm the presence of pentacyclic triterpenoids, a significant challenge persists in differentiating between betulin and ursane families. This differentiation is crucial for further analyses, as their inherent bond similarities make the identification process complex and elusive. Both families exhibit highly similar functional groups, leading to overlapping IR absorption bands that hinder straightforward differentiation. Advanced spectral deconvolution techniques, such as two-dimensional correlation spectroscopy or computational quantum chemistry, can enhance resolution and distinguish between these compounds [47]. Additionally, the elementary analysis provides further structural insights by quantifying the elemental composition, offering molecular-level data that reinforces spectral findings [48]. This approach is particularly useful for differentiating closely related triterpenoids. Complementary techniques like nuclear magnetic resonance (NMR) spectroscopy and mass spectrometry (MS) further refine structural identification by detecting characteristic molecular fragments

[49]. Integrating these methodologies enables precise classification of pentacyclic triterpenoids, facilitating comprehensive analyses and deeper exploration of their pharmacological properties.

3.1.2. Elemental analysis

Elemental analysis was performed to determine the isolated compounds' carbon, hydrogen, and oxygen composition. This technique provides essential molecular-level data that supports structural elucidation and differentiation of triterpenoid families. The calculated elemental analysis for compound **1** revealed a composition of 76.684 % carbon (C), 8.731 % hydrogen (H), and 14.583 % oxygen (O). Compound **2** exhibited a slightly higher carbon content of 79.413 %, along with 9.651 % hydrogen and 10.931 % oxygen. Similarly, compounds **3** and **3′** contained 79.228/79.239 % carbon, 10.201–10.192 % hydrogen, and 10.557–10.561 % oxygen. Compound **4** demonstrated the highest carbon percentage at 79.789 %, with 9.915 % hydrogen and 10.282 % oxygen. These results align with the FTIR findings, as variations in oxygen content correlate with the presence of hydroxyl and carbonyl functional groups, which were identified in the vibrational spectra.

Carbon and hydrogen composition differences further indicate structural variations between the isolated triterpenoids, supporting their classification within distinct pentacyclic families. This highlights the importance of combining elemental analysis with spectroscopic techniques to achieve a more comprehensive molecular characterization. Compared to the literature, De Jesus et al. [50] demonstrated that elemental analysis is reliable for confirming the purity of studied triterpenes, with reported purities exceeding 99.5 %. Similarly, Verardo et al. [51] utilised elemental analysis to verify the purity of newly isolated triterpenic acids, reinforcing its role in structural confirmation. This method plays a crucial role in verifying the identity and purity of these chemical entities, ensuring consistency with spectroscopic findings. Based on these results, NMR spectroscopy and UHPLC-MS will provide further insights into molecular connectivity and fragmentation patterns, which are essential for precise structural confirmation.

3.1.3. Chemical structure elucidation

3.1.3.1. Structural framework determination. Compound **1** was isolated as a white amorphous powder, with the molecular formula $C_{28}H_{38}O_4$, identified using the UHPLC-MS/MS technique at *m/z* 437.26 $[M\text{-}H]^-$. The ^{1}H NMR spectrum of compound **1** (Fig. 3**(a)**) showed two singlet methyl groups (δ_H 0.77 and 1.48), a methyl group doublet [δ_H 1.33 (3H, d)], two olefinic protons [(δ_H 5.17(1H, t) and 5.13 (1H, t], two couples of vinyl protons [δ_H 4.56 (1H, br s), 4.69 (1H, br s), 4.67 (1H, br s), and 4.57 (1H, br s)], two oxygenated methines [δ_H 3.08 (1H, d) and 2.97 (1H, dddt)]. The HMBC and HSQC spectra (Fig. 3**(b, c)**) were initially analysed to determine the ^{13}C NMR data, revealing a total of 28 carbon signals consisting of three methyls, nine methylenes, eight methines (including two oxygenated carbons at δ_C 73.8 and 76.6, as well as two olefinic carbons at δ_C 121.4 and 124.5) and seven quaternary carbons (including four olefinic carbons) (Table 1). An in-depth examination of the ^{2}D NMR spectra of compound **1**, particularly ^{1}H-^{1}H COSY, HMBC, and HSQC, enabled the identification of the structure. In the HMBC spectrum of compound **1**, the notable blue bonds illustrate extensive long-range correlations from 1H to 1 and 1H- 3 to C4; 1H-23 to C3; 1H-2 to C10; 3H-25 to C2, C5, C10 and C9; 3H-26 to C9, C7, C8, and C14; 3H-29 to C18 and C19; 1H-30 to C19 and C20 established the nor-ursane

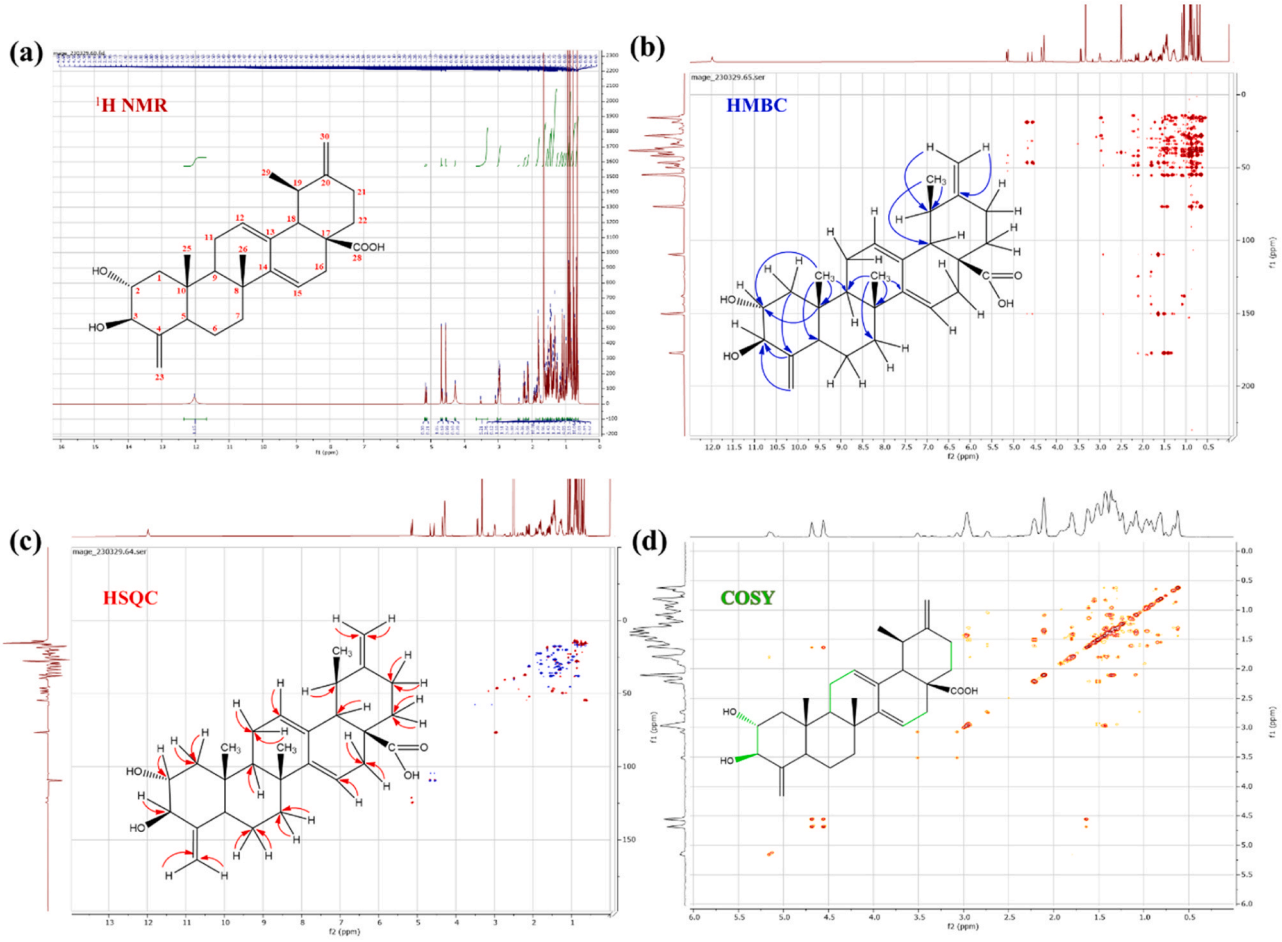

Fig. 3. (a) ^{1}H NMR spectra and (b) HMBC, (c) HSQC and (d) ^{1}H-^{1}H COSY correlations of the isolated compound 1.

Table 1
^{13}C NMR and ^{1}H NMR data of the purified compounds from the crude extract of rosemary solid waste.

Position	1		2		3		3'		4	
	δ_C	δ_H	δ_C	δ_H	δ_C	δ_H	δ_C	δ_H	δ_C	δ_H
1	46.5	1.24; 1.49	38.0	1.53	38.7	1.53	38.6	1.53; 0.90	38.7	1.53
2	73.8	3.08	26.8	1.44	27.4	1.45	27.0	1.45	27.4	1.45
3	76.6	2,97	76.7	3.0	76.7	3.00	76.8	3.00	76.7	3.00
4	150.2	-	38.3	-	38.3	-	38.3	-	38.1	-
5	54.9	2,18	54.7	2.17	54.9	2.18	54.8	2.18	54.7	2.18
6	28.0	1.38; 1.41	17.7	1.47; 1.31	150.2	-	18.3	1.31; 1.47	18.4	1.31;1.47
7	38.8	1.31; 1.74	36.0	1.52	46.1	1.61	36.7	1.58; 1.43	36.7	1.52;1.58
8	37.8	-	41.5	-	38.1	-	41.6	-	41.5	-
9	50.3	1.24	46.8	1.47	55.2	0.68	47.4	1.47	47.4	1.47
10	38.4	-	39.0	-	36.4	-	39.0	-	39.0	-
11	23.3	1.85; 1.93	27.3	1.8	23.2	1.85; 147	27.9	1.8; 1.93	28.0	1.8; 1.93
12	121.4	5.16	121.3	5.16	124.5	5.16	124.5	5.13	124.4	5.13
13	138.1	-	138.1	-	138.1	-	138.1	-	138.1	-
14	143.7	-	143.7	-	46.9	-	44.5	-	44.5	-
15	124.5	5.13	124.5	5.13	29.5	1.24; 1.09	30.6	1.28; 1.43		
16	32.1	2.12; 2.28	23.5	1.52; 1.94	24.2	1.94; 1.61	24.1	1.94; 1.52	24.2	1.94; 1.52
17	46.9	-	46.7	-	48.4	-	47.0	-	47.0	-
18	52.8	2.11	52.2	2.10	52.2	2.11	52.7	2.11	52.8	2.11
19	37.1	2.33	36.4	2.32	37.0	2.33	37.0	2.33	37.0	2.33
20	152.8	-	152.9	-	152.9	-	152.9	-	152.8	-
21	32.1	2.12; 2.28	31.6	2.14	32.2	2.15; 2.28	32.1	2.15; 2.28	32.2	2.15; 2.28
22	39.0	1.31; 1.74	40.5	2.73	39.0	1.31; 1.74	38.8	1,74; 1.31	38.9	1.31;
23	110.1	4.56; 4.69	28.1	0.9	23,7	1.05	28.6	0.9	28.7	0.9
24	-	-	15.8	0.67	16.5	0.68	16.4	0.68	16.5	0.68
25	15.7	0.77	16.6	0.75	17.1	0.93	17.2	0.75	16.5	0.93
26	23.0	1.48	18.3	1.05	19.3	1.61	17.3	0.82	17.3	0.75
27	-	-	-	-	26.6	1.10	23.5	1.10	23.6	1.10
28	177.2	-	178.2	-	178.2	-	178.2	-	178.2	-
29	18.4	1.33	18.4	1.4	18.4	1.31	18.3	1.31	19.0	1.31
30	105.1	4.67; 4.57	104.5	4.53; 4.67	105.2	4.57; 4.67	105.2	4,57; 4.67	105.2	4.57; 4.67
31	110.1	4.56; 4.69	-	-	110.1	4.56; 4.69	-	-	-	-

basic structure.

Further, in the ^{1}H-^{1}H COSY spectrum (Fig. 3**(d)**) of **1**, the submerged bold green lines indicate the range of correlations from H-2 through OH to H-3 through OH, H-9 to H-11 through H-12, H-15 to H-16, and H-21 to H-22 were instituted. Based on the coupling constant of H-2 and H-3 at δ_H 3.08 (d, $J = 10.9$ Hz) and 2.97 (dddt, $J = 20.1$, 16.0, 10.9, 4.9 Hz), it was concluded that HO-2 and HO-3 were in α and β configuration, respectively [13,15]. Compound **2** was purified as a white crystal. Its molecular formula, $C_{29}H_{42}O_3$, was inferred from UHPLC-MS/MS analysis at *m/z* 437.28 $[M\text{-}H]^-$. The ^{1}H NMR spectrum (Fig. 4**(a)**) of **2** displayed four singlet methyl groups (δ_H 0.9, 0.67, 0.75 and 1.05), a doublet of methyl group [δ_H 1.4 (3H, d)], two olefinic protons [(δ_H 5.17 (1H, t) and 5.13 (1H, t)], a pair of vinyl protons [δ_H 4.58; (1H, br s) and 4.67 (1H, br s)], and a methine carbon bonded to oxygen [δ_H 3.01(1H, dtd)]. The ^{13}C NMR data (Table 1) revealed a total of 29 carbon signals, consisting of five methyls, nine methylenes, and seven methines (including one oxygenated carbon at δ_C 76.7 and two olefinic carbons at δ_C 121.3 and 124.5), along with seven quaternary carbons (including three olefinic carbons), as determined from the HMBC and HSQC spectra (Fig. 4**(b, c)**). An in-depth examination of the ^{2}D NMR spectroscopy data of compound **2**, particularly ^{1}H-^{1}H COSY, HMBC, and HSQC, enabled the identification of the structure. In the HMBC spectroscopy data of compound **2**, the notable blue bonds illustrate extensive long-range correlations from 3H to 23 to C24; 1H(OH)-C2 and C4; 3H-25 to C2, C5, C10 and C9; 3H-26 to C9, C7, C8, and C14; 3H-29 to C18 and C19; 1H-30 to C19 and C20 confirmed the nor-ursane fundamental structure. Further, In ^{1}H-^{1}H COSY spectra (Fig. 4**(d)**) of compound **2**, the submerged bold green lines indicate the range of correlations from H-2 to H-3 through OH; H-9 to H-11 through H-12; H-15 to H-16; H-21 to H-22 were instituted. Following the findings in the literature [52], the constant coupling of H-3 at δ_H 3.01 (dtd, J=10.9, 5.2, 2.1 Hz) led to the conclusion that HO-3 was in the β configuration.

Compounds **3** and **3'** were purified in two different forms, of which **3** was crystalline and **3'** was amorphous. Its molecular formula, $C_{30}H_{46}O_3$, was inferred from UHPLC-MS/MS analysis at *m/z* 453.33 and 453.35 $[M\text{-}H]^-$, respectively. The ^{1}H NMR spectroscopy data of compounds **3** (Fig. 5**(a)**) and **3'** displayed five singlet methyl groups (δ_H 0.90, 0.68, 0.75–0.93, 0.82–0.75 and 1.10), a doublet of methyl group [δ_H 1.31 (3H, d)], one olefinic proton (δ_H 5.13 (1H, t), a pair of vinyl protons [δ_H 4.58; (1H, br s) and 4.67 (1H, br s)], and a methine carbon bonded to oxygen [δ_H 3.0 (1H, dt)]. The ^{13}C NMR data was identified from the HMBC and HSQC spectra, shown in Fig. 5**(b)** and Fig. 5**(c)**, indicating the presence of 30 carbon signals. Signals of the latter were identified as six methyls, ten methylenes, six methines, including one oxygenated carbon at δ_C 76.7 and one olefinic carbon at δ_C 124.4 and seven quaternary carbons, including two olefinic carbons, as depicted in Table 1. The ^{2}D NMR spectra of compounds **3** and **3'**, in particular, ^{1}H-^{1}H COSY, HMBC, and HSQC, gave an in-depth examination, enabling its structure to be identified. In the HMBC spectrum of compounds **3** and **3'**, the correlations are the same as compound **2,** except the existence of another correlation from 3H to 27 to C8, C14, C15, and C13 which establishes the nor-ursane basic structure. Further, the ^{1}H-^{1}H COSY spectra of compound **3** (Fig. 5**(d)**) and **3'** are the same as those of compound **2**.

Compound **4** was isolated as a white, shapeless powder. The molecular formula was determined as $C_{31}H_{46}O_3$ based on the UHPLC-MS/MS at *m/z* 465.33 $[M\text{-}H]^-$. The ^{1}H NMR spectrum (Fig. 6**(a)**) of compound **4** exhibited five singlet methyl groups (δ_H 1.05, 0.68, 0.93, 0.61 and 1.10), a doublet of methyl group [δ_H 1.33 (3H, d)], one olefinic proton δ_H 5.13 (1H, t), two couple of vinyl protons [δ_H 4.56 (1H, br s), 4.69(1H, br s), 4.67(1H, br s), and 4.57 (1H, br s)], and a methine carbon bonded to oxygen [δ_H 3.0 (1H, dt)]. The HMBC and HSQC spectra (Fig. 6 **(b)** and Fig. 6**(c)**) were initially analysed to interpret the ^{13}C NMR data, revealing a total of 31 carbon signals. These signals were categorised as six methyls, ten methylenes, and five methines (which included one oxygenated carbon at δ_C 76.6 and one olefinic carbon at δ_C 124.5), as well as eight quaternary carbons (including three olefinic carbons), as shown in Table 1. An in-depth examination of the ^{2}D NMR spectra of compound **4**, particularly ^{1}H-^{1}H COSY, HMBC, and HSQC, enabled the

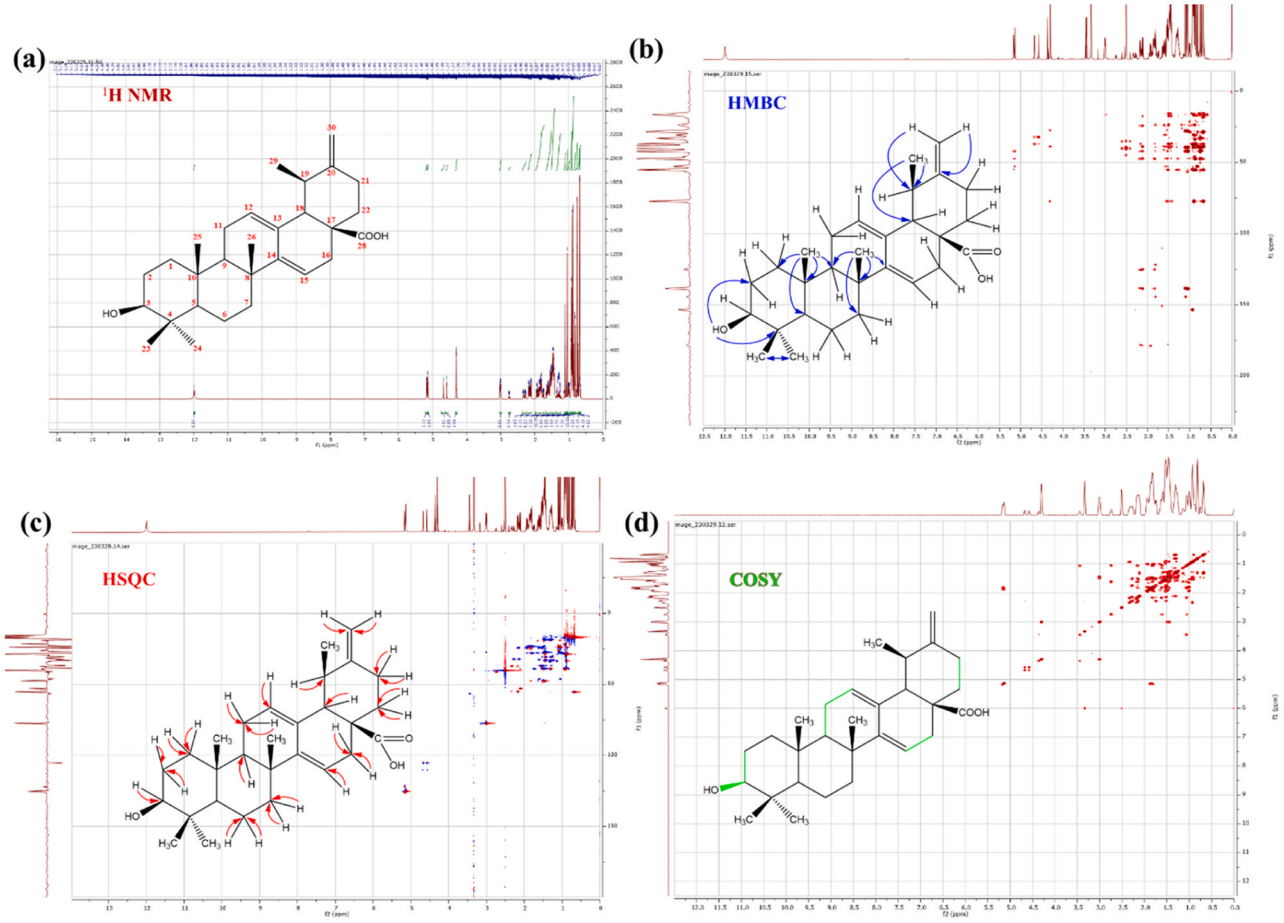

Fig. 4. (a) ^{1}H NMR spectra and (b) HMBC, (c) HSQC and (d) ^{1}H-^{1}H COSY correlations of the isolated compound 2.

identification of the structure. In the HMBC spectrum of compound **4**, the correlations are the same as for compounds **3** and **5**, except for another correlation from 1H to 31 to C4, which confirms the nor-ursane base structure [53]. Further, the ^{1}H-^{1}H COSY spectrum of compound **4** (Fig. 6**(d)**) is the same as compounds **2**, **3,** and **3**'.

Comparative structure determination with allied nor-ursane triterpenoids reported in the literature revealed that all four compounds had the typical 24-nor-ursane skeleton as previously reported. Despite this common structure, the isolated compounds show considerable structural variations. Compound **1** contained an additional hydroxyl group at C-2 in the α-configuration to a 24-nor-ursane-type triterpenoid previously isolated from the same waste plant material [22]. Another study also referred to its feature of extra olefinic and vinyl protons, as against the usually saturated analogues [13]. Compound **2**, although almost identical to micromeric acid, contained an extra double bond at C-14, which is a delicate but significant variation of the core structure. Compounds **3** and **3**′ also exhibited strong structural similarity to micromeric acid [54]. Compound **4**, which retained the nor-ursane skeleton, lacked one olefinic proton at C-14 from our earlier isolate from the same plant residue [22], suggesting a more saturated character. Though minor, such differences have profound effects on the physicochemical character and bioactivities of the triterpenoids, further enriching the structural diversity within this subclass.

3.1.3.2. Chiral configuration modelling. Following stereochemical analysis using Schrödinger's Maestro software, the absolute configurations of Compounds **1–4** were successfully assigned by 3D structural visualization and application of Cahn–Ingold–Prelog (CIP) priority rules (Fig. 7). The compounds were first passed through the LigPrep module to generate stereoisomers and optimize the geometry, enabling easy visualisation of the spatial arrangement of atoms around each chiral center. Compound **1** had an (*R*) configuration at C-2, C-3, C-8, C-10, and C-19, and an (*S*) configuration at C-17. Compound **2** had an (*R*)-configuration at C-8, C-10, and C-19, and an (*S*) configuration at C-3, and C-17. Compound **3** had the same (*R*) configuration at C-8, C-10, and C-19, along with an (*S*) configuration at C-3, C-14, and C-17. Similarly, compound **4**, was identical to compound **3** in terms of its stereochemical profile, with an (*R*) configuration at C-8, C-10, and C-19, and an (*S*) configuration at C-3, C-14, and C-17. For all four compounds, the invariant (*R*) configurations at C-8, C-10, and C-19, coupled with an (*S*) configuration at C-17, demonstrate a conserved stereochemical core, suggesting that these centres may play a fundamental role in the conformational stability of the compounds or their potential biological activity.

However, stereochemical variations at other positions, such as C-2, C-3, and C-14, can introduce stereochemical variations that alter molecular recognition in docking or interaction assays. Compound 1 has the most significant number of (R) configurations, including at the C-2 and C-3 positions, and has the most rigid chiral conformation. In contrast, compounds 3 and 4 have the same configurations and can be used as stereoisomeric controls. These results highlight the importance of correct stereochemical assignment before molecular modelling and establish a solid basis for exploring structure-activity relationships in future computational research. In support of this approach, Cinar et al. [55] and Wang et al. [56] both demonstrated the capability of computer calculations for stereochemical analysis. Cinar's analysis of Diels–Alder adducts accurately predicted the major and minor diastereomers, which were verified by ^{1}H NMR shifts [55]. Wang et al. [56] used DP4plus calculations along with spectroscopic and crystallographic data to

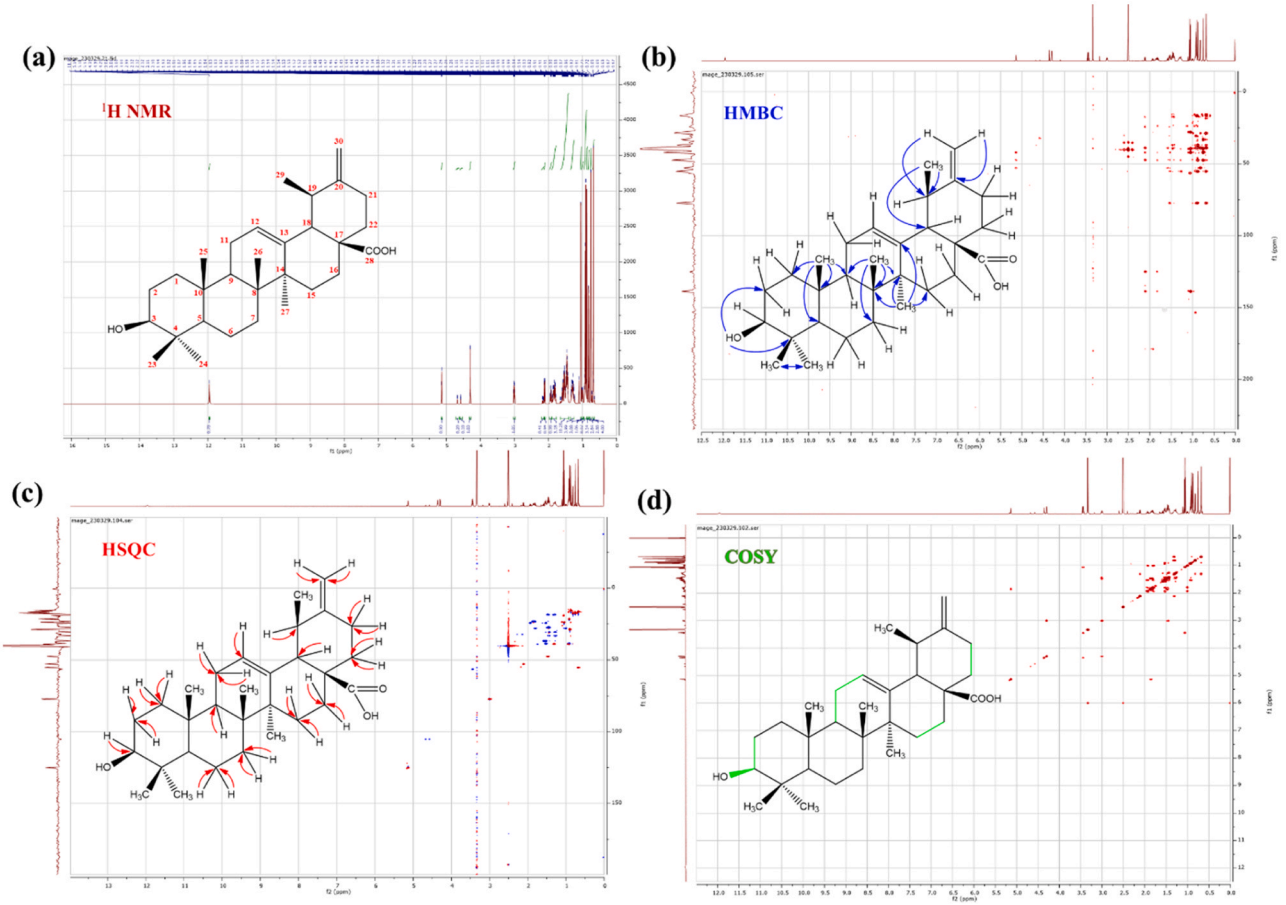

Fig. 5. (a) ^{1}H NMR spectra and (b) HMBC, (c) HSQC and (d) ^{1}H-^{1}H COSY correlations of the isolated compound 3.

determine the absolute configuration of Achroacid, a triterpenoid from *Achyrocline satureioides*. Together, these studies emphasize the validity of blending computational techniques and experimental techniques to resolve complex stereochemical configurations of synthetic and naturally occurring products.

3.2. Pathogen-fighting ability evaluation

The antibacterial activity of the isolated compounds and crude extracts derived from the solid waste of *R. tournefortii* de Noé was assessed and compared to the positive control. The positive control exhibited the highest inhibition across all tested microorganisms, with inhibition diameters ranging from 21.5 mm to 28.2 mm. While the inhibition zones of the extracts and isolated compounds were lower, they still demonstrated significant antimicrobial effects, emphasizing their potential as alternative bioactive agents. The results of the inhibition tests are summarized in Table 2. The extracts and isolated compounds exhibited varying degrees of inhibition compared to the positive control. The crude extracts demonstrated moderate antibacterial activity, with the ethyl acetate extract exhibiting more potent germicidal effects than the methanolic extract. The isolated compounds showed different antibacterial effects. Compound **1**, isolated from the methanolic extract, displayed significant inhibition against *E. coli* and *S. aureus*, with inhibition zones of 9.85 mm (vs. 8.75 mm) and 11.15 mm (vs. 9.95 mm), respectively.

According to the statistical analysis, the inhibition of compound **1** against *E. coli* and *S. aureus* was significantly greater than that of the methanolic extract ($p < 0.05$), as indicated by the different superscript letters in Table 2. The inhibitory effects of other derivatives, including compounds **2**, **3**, **3'**, and **4** from the ethyl acetate extract, also varied. For instance, compound **2** demonstrated superior inhibition against *E. coli* (10.2 mm compared to 9.75 mm for the crude extract), while its activity against *Geotrichum sp.* (10.7 mm) was also notable. Statistical analysis indicated that compound **2** showed a significant difference in inhibition against *E. coli* compared to the crude ethyl acetate extract ($p < 0.05$, with different statistical groups), but did not show significant differences against *Geotrichum sp.* or other strains. The molecular form plays a pivotal role in efficacy [57]. For example, compound **3'** in its amorphous form proved significantly more effective than its crystalline counterpart, compound **3**, due to several factors. Amorphous compounds generally have a larger specific surface area and enhanced solubility, facilitating the active substance's release and diffusion [58]. Furthermore, these forms demonstrate a greater capacity to interact with cell membranes, disrupting their structure and thereby enhancing their antimicrobial efficacy [59]. The statistical analysis confirmed that compound **3'** was significantly more effective against *Rhodotorula glutinis* (16.7 mm) than compound **3** (11.7 mm), with a p-value less than 0.05. However, it is important to note that the presumed amorphous nature of compound 3′ is inferred based solely on differences in biological activity. This interpretation was not confirmed by physicochemical techniques such as differential scanning calorimetry (DSC) or powder X-ray diffraction (PXRD). As such, the assignment of crystalline versus amorphous form remains speculative. Future studies incorporating solid-state characterization will be essential to validate this hypothesis and more accurately correlate physical form with observed bioactivity.

For instance, the methanolic extract effectively inhibited mould growth, while the ethyl acetate extract exhibited no inhibitory effects. Compounds **1** and **2** compromised the integrity of the fungal membrane, leading to increased permeability and subsequent cell lysis. Additionally, norursane-type pentacyclic triterpenoids, such as compounds **3'**, **2**,

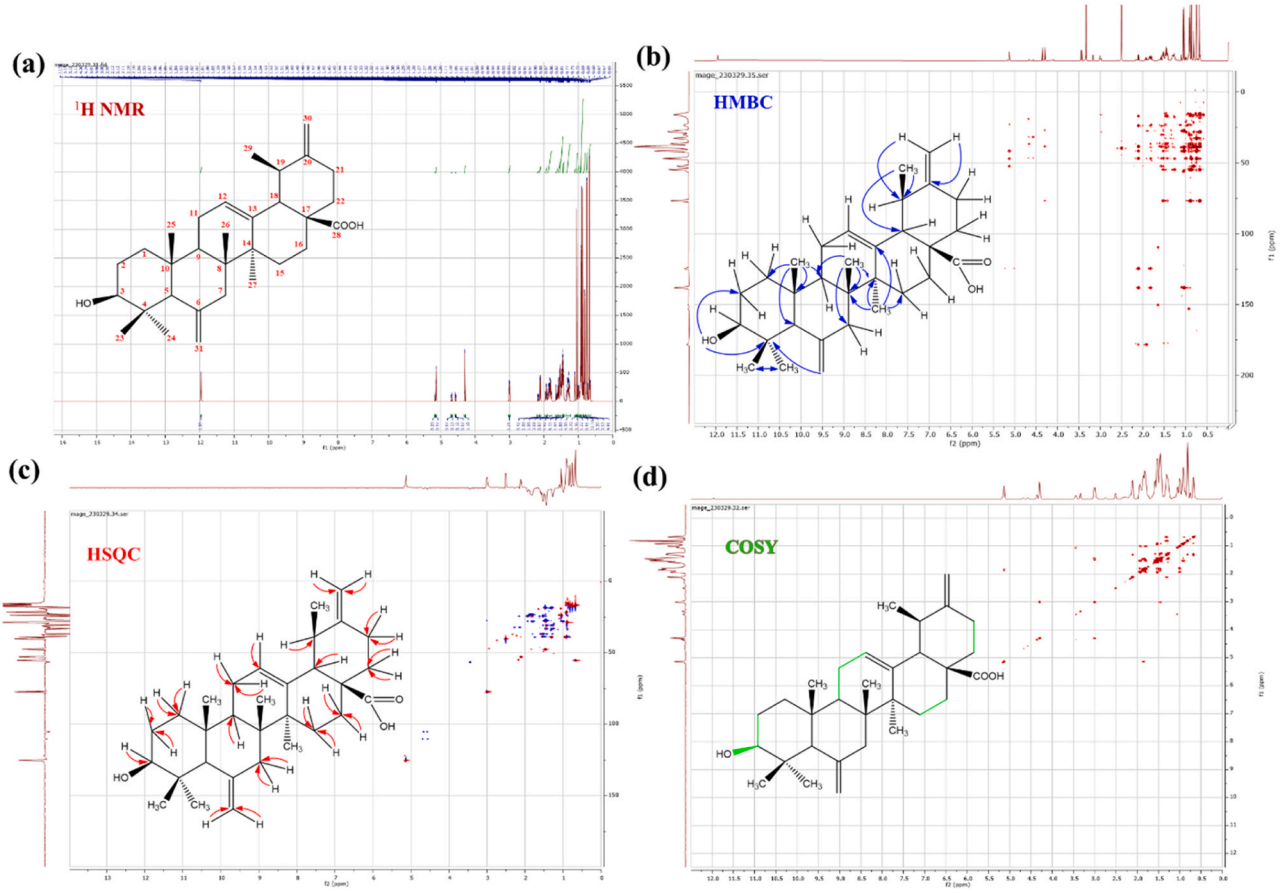

Fig. 6. (a) ^{1}H NMR spectra and (b) HMBC, (c) HSQC and (d) ^{1}H-^{1}H COSY correlations of the isolated compound 4.

and **1**, exert their antifungal activity by targeting ergosterol in the fungal cell membrane. This interaction induces membrane fluidity and permeability alterations, ultimately leading to pore formation [60]. Statistical results confirmed significant differences in inhibition between compound **1** and the crude methanolic extract for fungi such as *Penicillium* (9.85 mm vs. 9.55 mm for the methanolic extract, $p < 0.05$), showing that compound **1** is a more effective agent against fungi. Notably, compound **3'** exhibited substantial inhibition against *Rhodotorula glutinis* (16.7 mm), compared to 17.3 mm for the crude extract, suggesting that purification did not significantly enhance activity against this yeast. This result was not statistically significant, indicating that the purification process had a negligible effect on the activity against this particular yeast ($p \geq 0.05$). Furthermore, compound **1** demonstrated the highest activity against *Penicillium*, producing an inhibition zone of approximately 9.85 mm. This efficacy can be attributed to the structural characteristics of compound **1**, which features a nor-ursane type D-ring with a double bond at C-14 and C-15, along with an additional hydroxyl functional group (OH) [61]. This group may facilitate hydrogen bonding and electrostatic interactions with mould targets, further enhancing its antimicrobial activities [62]. These findings underscore the antimicrobial potential of *R. tournefortii* de Noé solid waste extracts and their isolated compounds. The statistical analysis supports the hypothesis that the purified compounds, particularly compound **1**, compound **2**, and compound **3'**, exhibit stronger antimicrobial activities compared to the crude extracts, with several significant differences noted ($p < 0.05$).

3.3. Controlled skin pigmentation

One of the most prevalent mechanisms regulating skin pigmentation is the inhibition of tyrosinase, a key enzyme in melanin biosynthesis [56]. This study evaluates the inhibitory effects of rosemary solid waste extracts and their isolated compounds on mushroom tyrosinase, using the dopa-chromium formation system from L-Dopa to measure enzymatic activity. Fig. 8 compares the tyrosinase inhibition of crude extracts, isolated compounds, and the control inhibitor, kojic acid. Notably, all compounds purified from the ethyl acetate extract exhibited substantial inhibitory activity, outperforming the initial extract. Compounds **2**, **3**, and **4** were particularly potent tyrosinase inhibitors, with IC_{50} values of 0.299 ± 0.017 mg/mL, 0.301 ± 0.029 mg/mL, and 0.304 ± 0.036 mg/mL, respectively, as outlined in Table 3. Statistical analysis confirmed that these compounds were significantly more effective than ethyl acetate extract, with an IC_{50} of 0.421 ± 0.012 mg/mL ($p < 0.05$). On the other hand, Compound **1**, purified from the methanolic extract, showed an IC_{50} of 0.404 ± 0.020 mg/mL, significantly weaker than the methanolic extract (IC_{50} = 0.157 ± 0.008 mg/mL). Statistical analysis confirmed that Compound **1** ($p < 0.05$) was less effective than the methanolic extract. Compared to kojic acid, a well-established tyrosinase inhibitor with an IC50 of 0.104 ± 0.047 mg/mL. Compound **1** exhibited significantly lower inhibitory effects ($p < 0.05$). However, Compounds **2**, **3**, and **4** showed comparable potency to kojic acid ($p \geq 0.05$).

The efficacy of purified triterpenoids in inhibiting tyrosinase depends on their structural and functional characteristics. Hydroxyl groups can form hydrogen bonds with the enzyme's active site, obstructing substrate binding [63]. Similarly, carbonyl groups may interact with amino acid residues, modulating the enzyme's catalytic function. The positioning of double bonds is critical to the observed inhibitory effects. Compound **2** exhibits stronger inhibition than compound **3** due to the double bond between C-14 and C-15, which enhances interaction with the enzyme's active site. This structural rigidity facilitates binding to tyrosinase [64]. The distinction between the crystalline

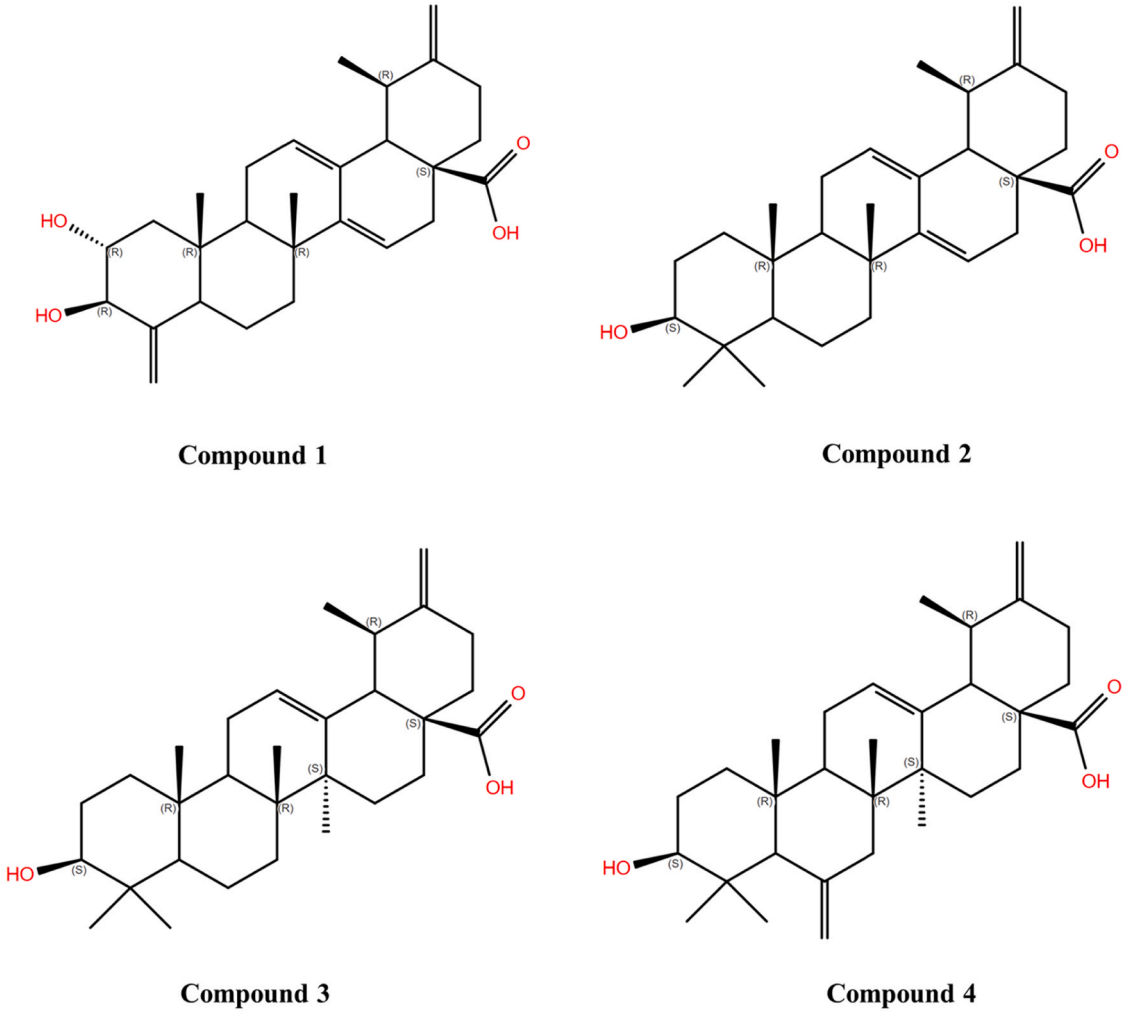

Fig. 7. Stereoisomer generation and chirality assignment of compounds 1–4 using LigPrep and Maestro visualisation.

Table 2
Antimicrobial performance of the isolated compounds from rosemary solid waste.

Samples	Inhibition diameter (mm)							
	Bacteria Gram -		Bacteria Gram+		Moulds		Yeasts	
	E. coli	*P. aeruginosa*	*L. innocua*	*S. aureus*	*Geotrichum sp.*	*A. niger*	*Penicillium*	*Rhodotorula glutinis*
Ext Meoh	8.75 ± 0.35^{d}	10.15 ± 0.21^{b}	9.2 ± 0.14^{bc}	9.95 ± 0.35^{c}	11.45 ± 1.20^{b}	-	10.15 ± 0.21^{b}	14.8 ± 0.32^{c}
1	9.85 ± 0.35^{bc}	9.9 ± 0.14^{bc}	9.7 ± 0.14^{ab}	11.15 ± 0.91^{b}	9.85 ± 0.21^{b}	-	9.5 ± 0.21^{b}	13.2 ± 0.24^{c}
Ext Act	9.75 ± 0.63^{bc}	10.15 ± 0.07^{b}	9.6 ± 0.14^{ab}	11.8 ± 0.28^{b}	-	-	-	17.3 ± 0.35^{b}
2	10.2 ± 0.28^{b}	9.35 ± 0.21^{c}	9.05 ± 0.07^{bc}	9.95 ± 0.07^{c}	10.7 ± 0.64^{b}	-	-	13.2 ± 0.15^{c}
3	10.3 ± 0.21^{b}	9.05 ± 0.07^{d}	8.35 ± 0.49^{c}	9.25 ± 0.13^{c}	-	-	-	11.7 ± 0.21^{b}
3’	10.35 ± 0.14^{b}	9.2 ± 0.28^{cd}	9.1 ± 0.14^{bc}	11.6 ± 0.28^{b}	-	-	-	16.7 ± 0.22^{b}
4	9.55 ± 0.63^{c}	9.85 ± 0.21^{bc}	9.2 ± 0.14^{bc}	9.25 ± 0.07^{c}	-	-	-	12.5 ± 0.36^{cd}
C^{+}	21.5 ± 0.25^{a}	22.6 ± 0.38^{a}	22.3 ± 0.96^{a}	22.6 ± 0.18^{a}	22.9 ± 0.36^{a}	21.8 ± 1.2^{a}	28.2 ± 1.16^{a}	22.8 ± 0.2^{a}

C^{+}; Cycloheximide served as a positive control for fungi, while gentamicin was utilised as a control for bacteria. Single superscript letters in each column indicate statistically significant differences between means ($p < 0.05$). Data are presented as means ± standard deviations ($n = 3$)

and amorphous forms of compounds **3** and **3’** further underscores the role of molecular conformation in inhibitory activity. The crystalline form of compound **3** (IC_{50}=0.301 ± 0.029 mg/mL) demonstrated greater inhibitory activity than its amorphous counterpart, compound **3’**. Suggesting that the crystalline structure provides an optimal geometry for enhanced interactions with the tyrosinase active site [65]. In contrast, the amorphous form may lead to less-defined molecular arrangements, potentially reducing its effectiveness [66].

Furthermore, positioning functional groups, such as hydroxyls and methyls, plays a critical role [67]. For instance, compound **4**, featuring a double bond at C-6 of the B ring, ranks third in inhibitory potency, highlighting the importance of steric effects and structural rigidity in enzymatic activity. Conversely, compound **1**, with an additional hydroxyl group, displayed the lowest inhibitory activity among the purified compounds (IC_{50}=0.404 ± 0.020 mg/mL). This reduced efficacy may be attributed to the absence of a methyl group at position C-24, which likely decreases its affinity for the enzyme’s active site. In conclusion, variations in inhibitory activities among the purified compounds reflect the intricate relationship between molecular structure and biological function. Understanding these structure-activity

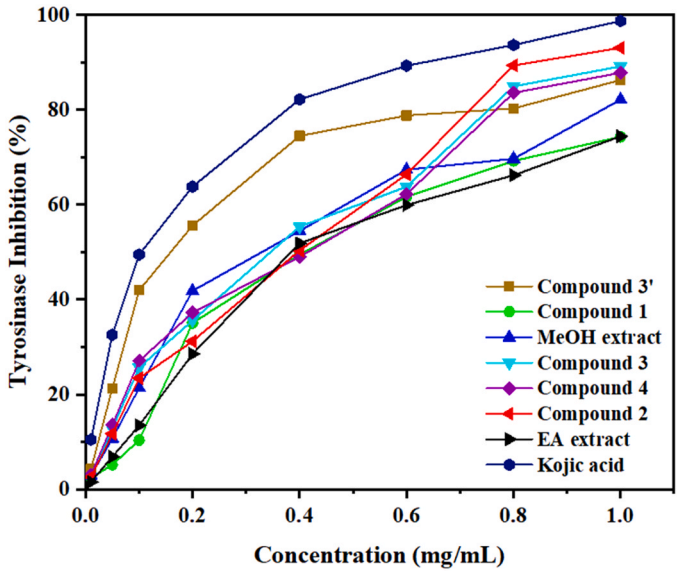

Fig. 8. Anti-tyrosinase potency of the isolated norursane-type triterpenoids from rosemary solid waste.

Table 3
IC_{50} values of norursane-type triterpenoids for tyrosinase inhibition.

Samples	IC_{50} (mg/mL)
MeOH extract	0.157 ± 0.008^{a}
Compound 1	0.404 ± 0.020^{c}
EA extract	0.421 ± 0.012^{c}
Compound 2	0.299 ± 0.017^{b}
Compound 3	0.301 ± 0.029^{b}
Compound 3′	0.321 ± 0.037^{b}
Compound 4	0.304 ± 0.036^{b}
Kojic acid	0.104 ± 0.047^{a}

Individual superscript letters in every column signify statistically significant differences among means ($p < 0.05$). Data are shown as means ± standard deviations ($n = 3$).

relationships is crucial for advancing rational drug design and developing effective pharmacological agents for treating hyperpigmentation in dermatological applications.

3.4. Molecular docking of isolated norursane-type triterpenoids

Molecular modelling plays a key role in studying the control of enzymes associated with carbohydrate digestion and pigmentation. Alpha-amylase and alpha-glucosidase, essential for the breakdown of starch and the conversion of carbohydrates into simple sugars, directly influence blood glucose levels, particularly in individuals with diabetes [68]. Inhibitors of these enzymes slow down carbohydrate digestion, thereby mitigating glycemic spikes. Similarly, tyrosinase, which catalyzes the production of melanin from L-tyrosine, is an important target in managing pigmentation disorders [69]. Therefore, the identification of compounds capable of inhibiting these enzymes offers therapeutic potential for treating metabolic and dermatological disorders. In this context, our study explored the inhibitory activity of compounds isolated from the solid waste of *R. tournefortii* de Noé using molecular docking simulations. These compounds favourably predicted interactions with alpha-amylase and alpha-glucosidase, even surpassing that of acarbose in terms of binding energy. Most compounds showed significant stability within the active site, with favourable binding energies, except for Compound **4**, which had a lower predicted affinity with the three studied proteins (Table 4). Negative and low docking scores confirm the robustness and relevance of the observed interactions. While negative and low docking scores suggest robust ligand-protein interactions, it is important to recognise that docking results are theoretical approximations. They do not always correlate directly with biological activity and must be interpreted cautiously.

In particular, Compound **1** exhibited the best stability within the active sites of alpha-amylase and alpha-glucosidase, with binding scores of −5.149 kcal/mol and −5.056 kcal/mol, respectively, significantly surpassing that of acarbose. These values suggest a potentially stronger binding affinity, positioning Compound **1** as a promising candidate for further investigation. For alpha-amylase, Compound **1** forms multiple interactions, including carbon-hydrogen bonds, pi-alkyl interactions, alkyl interactions, attractive charge interactions, and van der Waals interactions with the residues LEU156, TRP58, HIS30, LEU162, GLY306, HIS201, LYS200, and ILE235 (Fig. 9). For alpha-glucosidase, Compound **1** also forms various stabilising interactions, including hydrogen bonds with THR271, SER272, SER270, and THR739, as well as van der Waals interactions with the residues GLN255, LEU269, MET268, ASP741, PRO266, and TYR256 (Fig. 10).

Similarly, Compound **2** demonstrated stable predicted binding in the active site of tyrosinase, with a docking score of −5.880 kcal/mol, surpassing kojic acid. Its interactions with tyrosinase include conventional hydrogen bonds, pi-alkyl interactions, and van der Waals interactions with residues such as MET184, PHE197, ASN205, MET61, HIS60, and VAL218 (Fig. 11). These in silico results highlight the theoretical binding capabilities of the isolated compounds and offer a rationale for their potential as enzyme inhibitors. However, these predictions require experimental confirmation. Compound 1 is distinguished by an additional hydroxyl group and two exocyclic methylene groups, enhancing its ability to form hydrogen bonds and hydrophobic interactions with alpha-amylase and alpha-glucosidase, reinforcing its stability and inhibitory effectiveness. Compound **2**, alternatively, is better suited for inhibiting tyrosinase due to a structure that balances hydrogen and hydrophobic bonds, promoting an optimal fit in the enzyme's active site. These structural differences account for the variations in efficacy observed between the two compounds. Despite the superior docking scores of the isolated compounds, kojic acid exhibited the best inhibitory effect on tyrosinase in experimental assays. This discrepancy highlights the limitation of docking as a standalone predictor of biological activity. Factors such as solubility, bioavailability, and enzyme kinetics play critical roles in determining actual inhibitory potential [70].

For example, kojic acid's lower molecular weight and higher water solubility may enhance its interaction with tyrosinase under experimental conditions [71]. The literature shows norursane triterpenoids have demonstrated multifunctional potential in managing diabetes by inhibiting alpha-amylase, alpha-glucosidase, and tyrosinase enzymes. For example, pistagremic acid, with a docking score of −9.2 kcal/mol for alpha-glucosidase [69], forms stable hydrogen bonds due to its hydroxyl group at C-3 and carboxyl group at C-28 [69]. Compounds such as ilekudinol A and B, with docking scores of −8.5 and −8.7 kcal/mol for tyrosinase, respectively [72], highlight the role of specific functional groups in enhancing predicted binding. Nevertheless, while molecular

Table 4
Docking scores of the isolated compounds from rosemary solid waste docked with proteins (1B2Y), (5NN8), and (3NQ1) using SP docking.

N°	Compound Name	Docking score (kcal/mol)		
		Alpha-Amylase	Alpha-Glucosidase	Tyrosinase
1	Compound 1	−5.149	−5.056	−4.414
2	Compound 2	−4.985	−3.558	−5.880
3	Compound 3	−3.547	−3.920	−4.389
4	Compound 4	−3.507	−3.067	−3.148
5	Acarbose (standard)	−4.877	−4.925	–
6	Kojic acid (standard)	–	–	−4.888

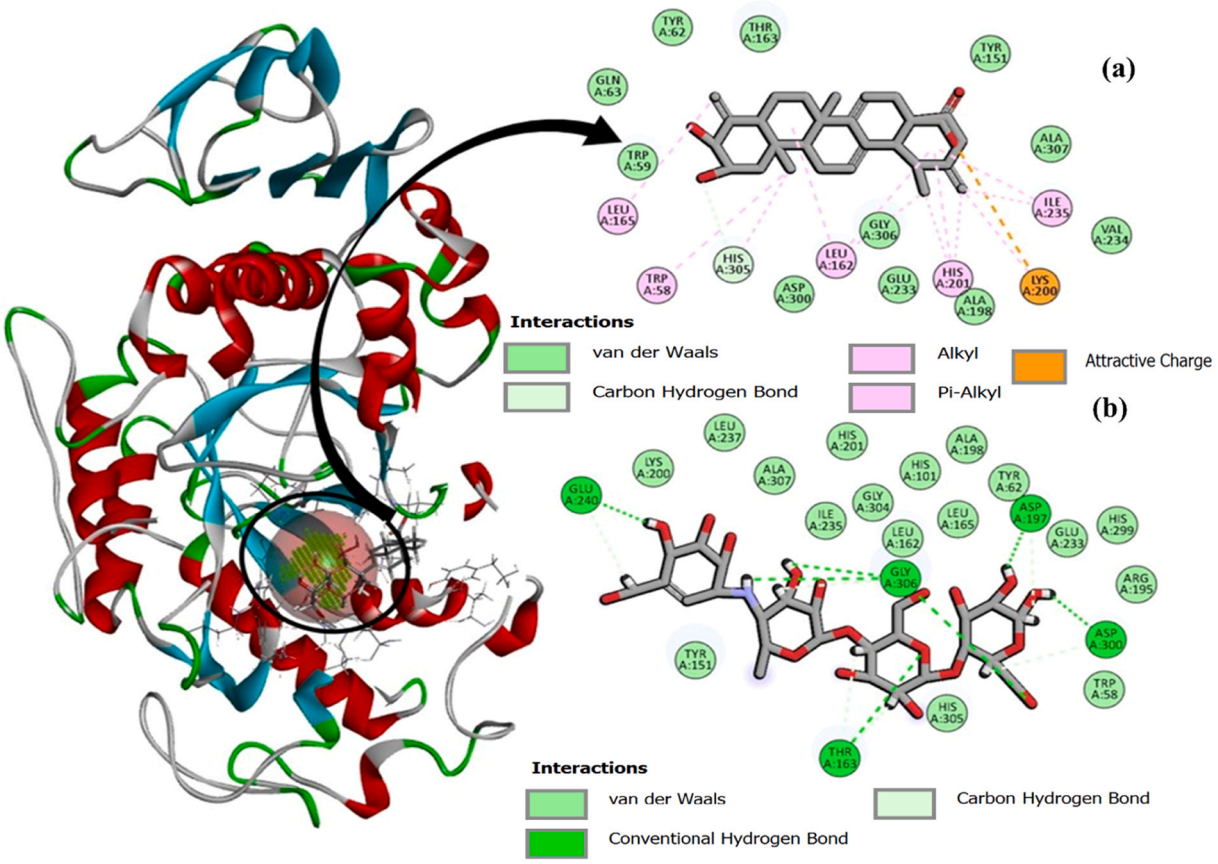

Fig. 9. 2D intermolecular interactions between; (a) Compound 1 and (b) Acarbose with the protein α-Amylase's active site (PDB: 1B2Y).

docking offers valuable preliminary insights, in vivo studies remain essential for confirming efficacy, safety, and pharmacokinetic properties. Future investigations, including clinical trials, are crucial to validating the therapeutic potential of these compounds.

3.5. Physicochemical limitations and real-world applicability

Although the compounds isolated from *R. tournefortii* de Noé solid waste show promising antimicrobial and tyrosinase inhibitory activities, their practical use is subject to certain physicochemical restrictions. Nor-ursane-type triterpenoids, which are poorly soluble in water and have low membrane permeability due to their high molecular weight and lipophilicity, are particularly susceptible to problems of bioavailability and absorption. For example, compound 1, while possessing good in vitro activity, exists as a poorly water-soluble compound, potentially limiting its biodistribution and therapeutic application in vivo. Similarly, compound 3′ was more active as an antimicrobial compound in its amorphous form. Still, the crystalline form was more active as a tyrosinase inhibitor, showing that different biological activities could favour physical forms. Although both forms were dissolved in ethanol before testing, the differences in bioactivity may still reflect the influence of the initial physical state. Amorphous and crystalline solids can differ in terms of dissolution kinetics, solvation and transient conformational states or aggregates in solution that influence drug-target interactions [73]. These subtle influences can affect the availability or presentation of functional groups at the biological interface. Therefore, even in solution, the initial physical form can indirectly impact pharmacological effects. Although we have not experimentally measured thermodynamic stability, it is well established that amorphous forms are generally less stable than crystalline forms. This can result in recrystallisation over time, affecting shelf life and presenting formulation challenges.

A further complication is the limited solubility of these compounds in aqueous media. Dissolution could only be achieved in ethanol with moderate heating—conditions unsuitable for many clinical or cosmetic formulations, where water-based systems are preferred for safety and ease of use. This dependence on ethanol poses problems of reproducibility and formulation scalability, making these compounds less attractive than active substances that are readily soluble under standard conditions. In addition, there is a considerable difference between computational docking predictions and in vitro activity. For example, kojic acid showed more effective tyrosinase inhibition in vitro than triterpenoids, whereas docking predictions showed the opposite. This highlights the limitations of in silico models for correctly predicting biological efficacy, particularly when physicochemical limitations such as solubility and access to enzymes exist. To overcome these limitations and fully exploit the potential of these drugs, advanced delivery methods, such as nanoencapsulation, inclusion complexes, or chemical derivatisation, may be required. These methods could optimise bioavailability, stabilise the substance, and improve systemic or local absorption. Finally, in vivo studies and formulation design will be important to establish efficacy and overcome obstacles that cannot be overcome alone by in vitro or computational means.

3.6. Challenges and future outlook

3.6.1. Enhancing the use of nor-ursane triterpenoids in porous food materials

Incorporating nor-ursane-type pentacyclic triterpenoids into porous materials for food packaging presents an innovative solution for enhancing food preservation and sustainability. Pentacyclic triterpenoids, known for their potent antimicrobial, antioxidant, and mechanical properties, these compounds offer a promising alternative to

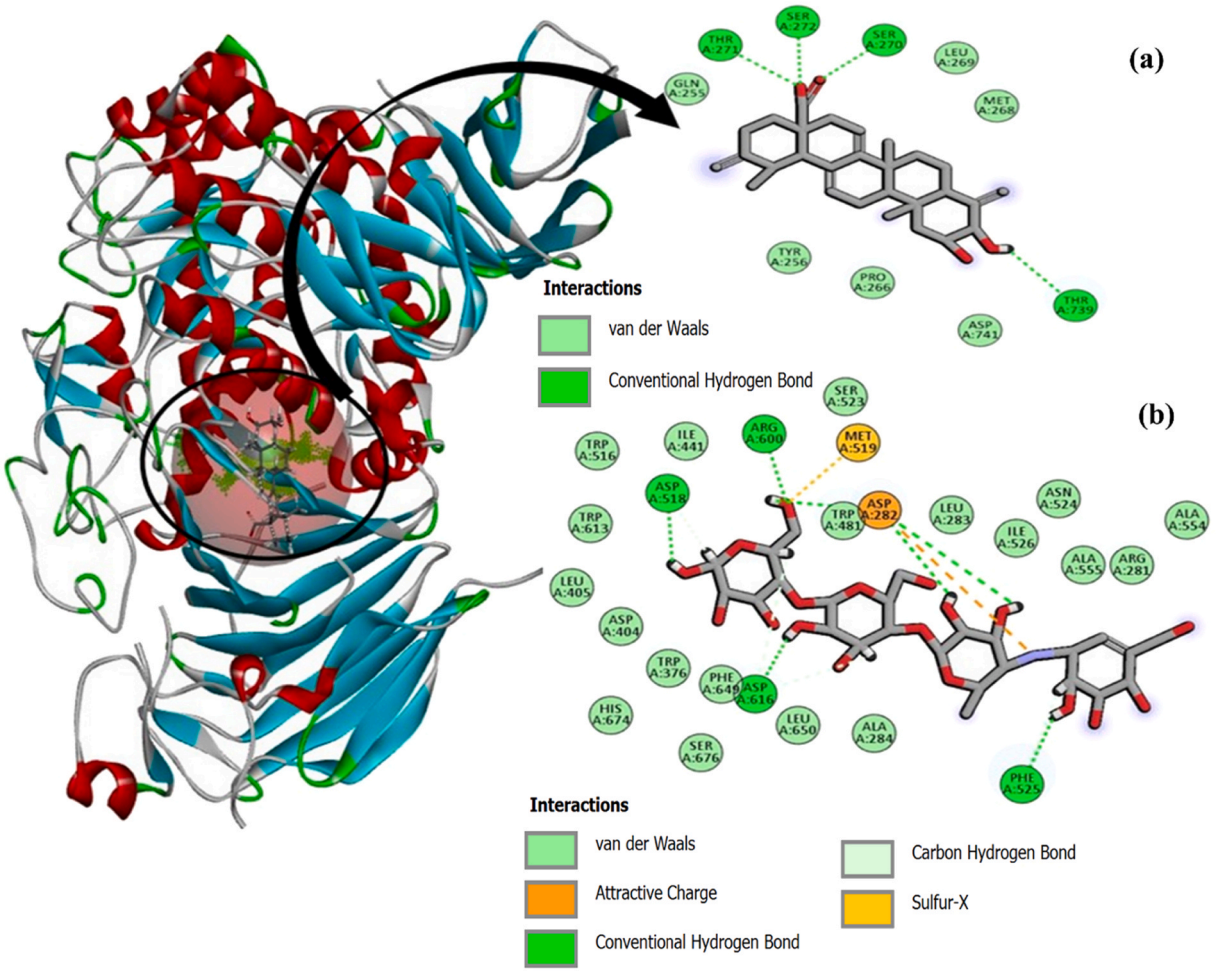

Fig. 10. 2D intermolecular interactions between; (a) Compound 1 and (b) Acarbose with the protein α-Glucosidase 's active site (PDB: 3NQ1).

traditional synthetic additives and non-biodegradable packaging materials [74]. Several studies have demonstrated the high efficacy of these triterpenoids, particularly when integrated into biodegradable films. For instance, incorporating plant extracts containing triterpenoid compounds into chitosan matrices has been associated with improved antibacterial efficacy against harmful pathogens like *Escherichia coli* and *Staphylococcus aureus* [75]. In addition, these films exhibit over 85 % DPPH radical scavenging activity, reflecting their strong antioxidant properties, which play a crucial role in protecting foods from oxidative damage and spoilage [17]. Beyond their biological activity, the mechanical properties of packaging materials are also enhanced by including these triterpenoids. Tensile strength tests have revealed that composite films containing triterpenoids can achieve 24.9 MPa, significantly higher than those of pure chitosan films. This improvement in strength makes them more durable and suitable for commercial food packaging, particularly for products requiring long shelf lives. Additionally, the water vapour permeability of these films remains within a favourable range [75], a key factor in preventing food dehydration and ensuring product freshness.

These promising laboratory findings suggest strong potential for bioactive packaging; however, translating these results into commercial practice presents several challenges. In practical food applications, certain bioactive-enriched materials have demonstrated significant impacts on product shelf life. For example, edible coatings enriched with plant-based extracts have been shown to extend the shelf life of strawberries by up to 15 days, in contrast to untreated produce, which spoils within 5–7 days [76]. Similarly, packaging materials used for meat products have achieved a 50 % reduction in microbial contamination during refrigerated storage, helping maintain product quality and safety for extended periods [77]. Moreover, some porous matrices have been reported to offer sustained antimicrobial activity for up to 30 days through controlled release mechanisms, highlighting their potential for long-term food preservation [78]. However, while these functional properties are promising, the practical application of nor-ursane triterpenoids faces significant hurdles. Extraction complexity is a primary challenge, as the current methods for isolating and purifying these compounds are both resource-intensive and costly. This undermines the environmental benefits of using natural triterpenoids, as energy and material consumption during extraction may negate the sustainability gains. Moreover, the lack of standardised, scalable extraction techniques means that commercial adoption remains limited. Developing more efficient and cost-effective extraction processes will be essential to enable broader implementation in the food packaging sector.

Another critical concern is the variability in the chemical properties of different triterpenoids, which may affect their behaviour in diverse food matrices. Factors such as pH, temperature, moisture levels, and food composition can influence the efficacy and stability of nor-ursane triterpenoids. For example, acidic environments might alter their antimicrobial activity, while temperature fluctuations could impact their controlled release from packaging materials [79]. Therefore, a comprehensive understanding of these interactions is necessary to optimise the use of nor-ursane triterpenoids in real-world food systems. Furthermore, while antimicrobial and antioxidant properties have been well-documented in controlled laboratory conditions, more extensive research is required to determine their long-term stability and effectiveness across various food products. This includes evaluating how

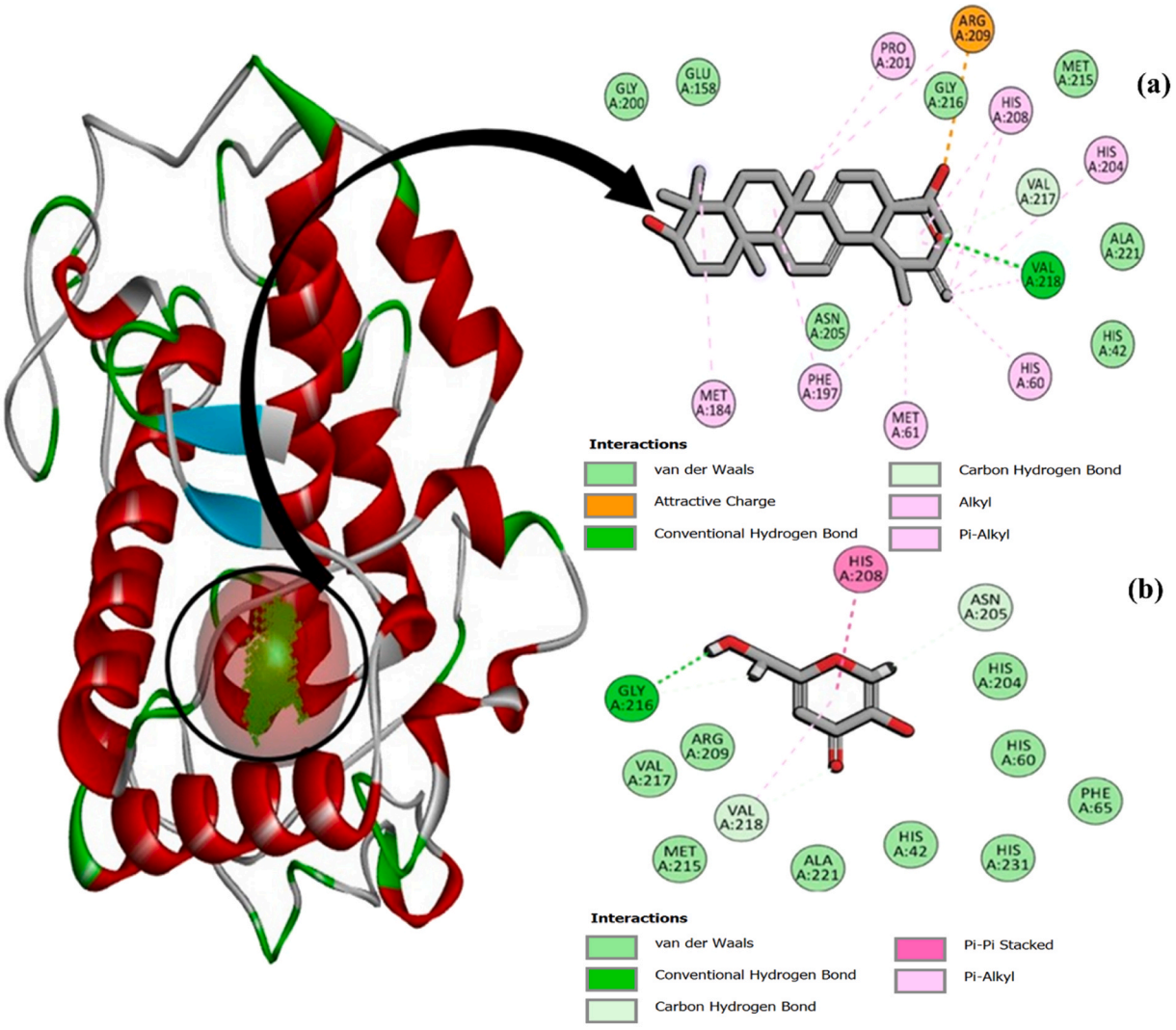

Fig. 11. 2D intermolecular interactions between; (a) compound 2 and (b) kojic acid with the protein tyrosinase's active site (PDB: 5NN8).

triterpenoids behave under commercial packaging conditions, such as during transportation and extended storage periods, which can present challenges not encountered in laboratory environments.

3.6.2. Sustainability and environmental benefits

Nor-ursane-infused porous materials also provide significant advantages in terms of environmental sustainability, positioning them as key players in the shift away from petroleum-based plastics. Biodegradability is one of their most notable features. While conventional plastics can persist in the environment for centuries, materials infused with natural extracts degrade much more rapidly, especially when incorporated into biodegradable polymer matrices like chitosan [80]. This presents a viable alternative to traditional plastics, comprising a significant portion of global plastic consumption, yet have a dismal recycling rate. The environmental urgency to reduce plastic waste is well-documented, with approximately 300 million tons of plastic waste generated annually [81]. Using natural, biodegradable alternatives such as nor-ursane triterpenoids could play a crucial role in mitigating this crisis. From a sustainability perspective, the antimicrobial properties of nor-ursane triterpenoids are particularly valuable. Studies on similar triterpenoids, such as betulin, have shown a 2–3 log reduction in microbial growth, extending the shelf life of perishable goods by up to 31 days [82]. This is especially relevant in the fight against global food waste, which accounts for nearly one-third of all food produced annually. The porous structure of materials infused with nor-ursane also facilitates gas exchange, which is critical for maintaining the freshness of fresh produce, further enhancing their value in food packaging applications.

Moreover, the growing consumer demand for eco-friendly products cannot be overlooked. With 66 % of global consumers indicating a willingness to pay a premium for environmentally sustainable options, the market potential for natural, biodegradable packaging solutions is substantial [83]. Nor-ursane triterpenoids, which combine environmental sustainability with functional benefits such as antimicrobial protection and enhanced packaging integrity, are well-positioned to meet this demand. From an economic standpoint, early estimates suggest that the cost of producing materials infused with natural extracts is only slightly higher than that of conventional polyethylene packaging, making it a feasible alternative for manufacturers [84]. Despite these advantages, some critical challenges remain. While natural extracts-infused materials have demonstrated biodegradability and mechanical strength in controlled environments, further real-world assessments are needed to confirm their degradation rates under typical environmental conditions. Additionally, while the slight increase in production costs may be acceptable for environmentally conscious consumers, price-sensitive markets and industries with narrow profit margins may find this a significant barrier to adoption. To achieve large-scale commercial success, it will be necessary to balance the

cost-benefit ratio, especially when scaling up production to meet rising demand.

In conclusion, nor-ursane-infused porous materials represent a powerful opportunity to address both food preservation and environmental sustainability in the packaging industry. Their ability to reduce microbial contamination, extend shelf life, and offer biodegradable alternatives to plastic packaging makes them a critical innovation in the shift toward a circular economy. However, their full potential can only be realised through further research into their long-term performance, more cost-effective extraction methods, and wider adoption across various food industries. With continued advancements, these materials could significantly contribute to reducing food spoilage and plastic waste, shaping a more sustainable future for global packaging solutions.

4. Conclusion

The developed nor-ursane-type triterpenoids were successfully purified using recrystallisation, offering a cost-effective and efficient alternative to conventional and advanced methodologies. Their molecular structures and chemical groups were analysed using cutting-edge spectroscopic techniques. These triterpenoids exhibited significant biological activities, including strong antimicrobial effects against pathogens such as *E. coli*, *S. aureus*, and *Geotrichum sp.*, and potent tyrosinase inhibition. Molecular docking studies revealed favourable binding interactions, particularly for compounds 1 and 2, which showed stability and potential as therapeutic agents against diabetes and pigmentation disorders. Despite these promising biological activities, several physicochemical challenges hinder their broader applicability. The compounds' poor solubility in water and low membrane permeability limit their bioavailability and therapeutic effectiveness, especially in in vivo applications. Moreover, the dissolution process, which requires ethanol and moderate heating, complicates formulation, making them less practical for clinical or cosmetic use. These physicochemical limitations, combined with discrepancies between in vitro and in vivo activity, highlight the need for addressing bioavailability and formulation stability in future studies. In the context of porous food materials, additional challenges arise, such as variability in performance across different food matrices and the need for long-term stability studies. While these triterpenoids offer significant promise in both medical and food packaging applications, further research is required to assess their stability, scalability, and practical efficacy. Overcoming these challenges could contribute to reducing plastic waste, enhancing food preservation, and advancing the development of sustainable solutions in various industries.

CRediT authorship contribution statement

Kadier Abudukeremu: Visualization, Validation, Investigation. **Bentouhami Nour Eddine:** Methodology, Investigation. **Sher Farooq:** Writing – review & editing, Project administration, Funding acquisition. **Fauconnier Marie-Laure:** Writing – review & editing, Supervision, Project administration, Investigation. **Merzouki Mohammed:** Methodology, Formal analysis. **Bouakline Hamza:** Visualization, Methodology, Formal analysis. **Ziani Imane:** Writing – review & editing, Writing – original draft, Methodology, Investigation, Funding acquisition, Formal analysis, Data curation, Conceptualization. **El Bachiri Ali:** Writing – review & editing, Validation, Supervision, Investigation, Conceptualization. **Challioui Allal:** Methodology, Investigation. **Asehraou Abdeslam:** Methodology, Investigation. **Ansar Sabah:** Writing – review & editing, Funding acquisition.

Declaration of Competing Interest

The authors state that they possess no financial conflicts of interest or personal connections that might have affected the research shown in this paper.

Acknowledgement

The authors convey their heartfelt thanks to Cluster Valbiom Maroc for supporting the project and recognising the financial help obtained from the International Society of Engineering Science and Technology (ISEST) UK. The authors extend their appreciation to the Researchers Supporting Project number (RSP2025R169), King Saud University, Riyadh, Saudi Arabia.

Data availability

Data will be made available on request.

References

[1] Z. Zhang, M.Z. Malik, A. Khan, N. Ali, S. Malik, M. Bilal, Environmental impacts of hazardous waste, and management strategies to reconcile circular economy and eco-sustainability, Sci. Total Environ. 807 (2022) 150856, https://doi.org/10.1016/j.scitotenv.2021.150856.
[2] B. Koul, M. Yakoob, M.P. Shah, Agricultural waste management strategies for environmental sustainability, Environ. Res. 206 (2022) 112285, https://doi.org/10.1016/j.envres.2021.112285.
[3] R.A. Sheldon, Engineering a more sustainable world through catalysis and green chemistry, J. R. Soc. Interface 13 (2016) 20160087, https://doi.org/10.1098/rsif.2016.0087.
[4] A.K. Rashwan, H. Bai, A.I. Osman, K.M. Eltohamy, Z. Chen, H.A. Younis, A. Al-Fatesh, D.W. Rooney, P.-S. Yap, Recycling food and agriculture by-products to mitigate climate change: a review, Environ. Chem. Lett. 21 (2023) 3351–3375, https://doi.org/10.1007/s10311-023-01639-6.
[5] A. Karnwal, T. Malik, Exploring the untapped potential of naturally occurring antimicrobial compounds: novel advancements in food preservation for enhanced safety and sustainability, Front. Sustain. Food Syst. 8 (2024) 1307210, https://doi.org/10.3389/fsufs.2024.1307210.
[6] J. Malik, S.C. Mandal, Pentacyclic triterpenoids: diversity, distribution and their propitious pharmacological potential, Phytochem. Rev. (2024) 1–33, https://doi.org/10.1007/s11101-024-10056-8.
[7] R.T.S. Frighetto, R.M. Welendorf, E.N. Nigro, N. Frighetto, A.C. Siani, Isolation of ursolic acid from apple peels by high speed counter-current chromatography, Food Chem. 106 (2008) 767–771, https://doi.org/10.1016/j.foodchem.2007.06.003.
[8] S.T. Cargnin, S.B. Gnoatto, Ursolic acid from apple pomace and traditional plants: a valuable triterpenoid with functional properties, Food Chem. 220 (2017) 477–489, https://doi.org/10.1016/j.foodchem.2016.10.029.
[9] C. Wang, X. Wang, S. Zhao, W. Sun, S. Tong, Preparative separation of structural isomeric pentacyclic triterpene oleanolic acid and ursolic acid from natural products by pH-zone-refining counter-current chromatography, RSC Adv. 9 (2019) 38860–38866, https://doi.org/10.1039/C9RA06082K.
[10] W. Luo, F.C.F. Ip, G. Fu, K. Cheung, Y. Tian, Y. Hu, A. Sinha, E.Y.L. Cheng, X. Wu, V. Bustos, A pentacyclic triterpene from Ligustrum lucidum targets γ-secretase, ACS Chem. Neurosci. 11 (2020) 2827–2835, https://doi.org/10.1021/acschemneuro.0c00389.
[11] L.A. Ticona, K. Slowing, A.M. Serban, M.H. Bastante, M.J. Hernáiz, Wound healing, anti-inflammatory and anti-melanogenic activities of ursane-type triterpenes from Semialarium mexicanum (Miers) Mennega, J. Ethnopharmacol. 289 (2022) 115009, https://doi.org/10.1016/j.jep.2022.115009.
[12] B.K. Harley, R.A. Dickson, I.K. Amponsah, I.O. Ben, D.W. Adongo, T.C. Fleischer, S. Habtemariam, Flavanols and triterpenoids from Myrianthus arboreus ameliorate hyperglycaemia in streptozotocin-induced diabetic rats possibly via glucose uptake enhancement and α-amylase inhibition, Biomed. Pharm. 132 (2020) 110847, https://doi.org/10.1016/j.biopha.2020.110847.
[13] H.R. Wu, X.F. He, X.J. Jin, H. Pan, Z.N. Shi, D.D. Xu, X.J. Yao, Y. Zhu, New nor-ursane type triterpenoids from Gelsemium elegans, Fitoterapia 106 (2015) 175–183, https://doi.org/10.1016/j.fitote.2015.09.002.
[14] W. Xu, J. Tan, Y. Mu, D. Zheng, X. Huang, L. Li, New antimicrobial terpenoids and phloroglucinol glucosides from Syzygium szemaoense, Bioorg. Chem. 103 (2020) 104242, https://doi.org/10.1016/j.bioorg.2020.104242.
[15] D.S. Jang, J.M. Kim, J.H. Kim, J.S. Kim, 24-nor-ursane type triterpenoids from the stems of Rumex japonicus, Chem. Pharm. Bull. 53 (2005) 1594–1596, https://doi.org/10.1248/cpb.53.1594.
[16] J.-S. Zhang, Y. Qian, Z.-Q. Xin, X.-X. Cao, Z. Yang, H. Zhang, Bioactive pentacyclic triterpenoids from the whole plants of Pterocephalus hookeri, Phytochemistry 195 (2022) 113040, https://doi.org/10.1016/j.phytochem.2021.113040.
[17] K. Qiu, S. Wang, F. Duan, Z. Sang, S. Wei, H. Liu, H. Tan, Rosemary: unrevealing an old aromatic crop as a new source of promising functional food additive—a review, Compr. Rev. Food Sci. Food Saf. 23 (2024) e13273, https://doi.org/10.1111/1541-4337.13273 https://doi.org/10.1111/1541-4337.13273.
[18] X.-J. Zhong, Z. Na, W. Xin, L.I. Jin-Jie, M.A. Hui, J. Yue, X.U. Jia-Hui, L.I.N. Peng-Cheng, X.-Y. Shang, Three new ursane-type triterpenoids from Rosmarinus officinalis and their biological activities, Chin. J. Nat. Med. 20 (2022) 155–160, https://doi.org/10.1016/S1875-5364(21)60103-6.
[19] N. Zhou, Z. yu Wang, Y. Wu, X. jian Zhong, X. Wang, J. jie Li, X. ya Shang, Norursane-type triterpenoids from Rosmarinus officinalis and their anti-

inflammatory activity evaluation, Fitoterapia 153 (2021) 104982, https://doi.org/10.1016/j.fitote.2021.104982.
[20] G. Altinier, S. Sosa, R.P. Aquino, T. Mencherini, R. Della Loggia, A. Tubaro, Characterization of topical anti-inflammatory compounds in Rosmarinus officinalis L, J. Agric. Food Chem. 55 (2007) 1718–1723, https://doi.org/10.1021/jf062610+.
[21] X. Chen, Q. Luo, W. Hu, J. Chen, R. Zhang, Labdane and isopimarane diterpenoids from Rosmarinus officinalis solid wastes: MS/MS spectrometric fragmentations and neuroprotective effect, Ind. Crops Prod. 177 (2022) 114441, https://doi.org/10.1016/j.indcrop.2021.114441.
[22] I. Ziani, H. Bouakline, M. Merzouki, M. Fauconnier, F. Sher, N.E. Bentouhami, A. Asehraou, A. El Bachiri, Purification of bioactive compounds from rosemary by-products for innovative solutions in food industry, Ind. Crops Prod. 223 (2025) 120125, https://doi.org/10.1016/j.indcrop.2024.120125.
[23] I. Ziani, H. Bouakline, M.I. Yahyaoui, Y. Belbachir, M.-L. Fauconnier, A. Asehraou, A. Tahani, A. Talhaoui, A. El Bachiri, The effect of ethanol/water concentration on phenolic composition, antioxidant, and antimicrobial activities of Rosmarinus tournefortii de Noé hydrodistillation solid residues, J. Food Meas. Charact. 17 (2023) 1602–1615, https://doi.org/10.1007/s11694-022-01722-6.
[24] I. Ziani, H. Bouakline, S. Bouknana, N.E. Bentouhami, F. Sher, S. Ansar, M.-L. Fauconnier, M. Bnouham, A. El Bachiri, Sustainable management of rosemary wastewater and essential oil in agri-environmental bioprocessing, Food Biosci. 62 (2024) 105263, https://doi.org/10.1016/j.fbio.2024.105263.
[25] G. Yang, Z. Qi, S. Shan, D. Xie, X. Tan, Advances in separation, biological properties, and structure–activity relationship of triterpenoids derived from camellia oleifera abel, J. Agric. Food Chem. 72 (2024) 4574–4586, https://doi.org/10.1021/acs.jafc.3c09168.
[26] S. Agatonovic-Kustrin, S. Wong, A.V. Dolzhenko, V. Gegechkori, D.W. Morton, HPTLC-guided flash chromatographic isolation and spectroscopic identification of bioactive compounds from olive flowers, J. Chromatogr. A 1735 (2024) 465310, https://doi.org/10.1016/j.chroma.2024.465310.
[27] I. Ziani, A. El Guerraf, N.E. Bentouhami, M. Brahmi, H. Bouakline, A. El Bachiri, M.-L. Fauconnier, S. Ansar, F. Sher, Nanoreinforcement strategies for enhancing biodegradable composites in biochemical applications within agriwaste valorisation, Biocatal. Agric. Biotechnol. 58 (2024) 103223, https://doi.org/10.1016/j.bcab.2024.103223.
[28] M. Elyashberg, Identification and structure elucidation by NMR spectroscopy, TrAC - Trends Anal. Chem. 69 (2015) 88–97, https://doi.org/10.1016/j.trac.2015.02.014.
[29] J.-H. Ruan, J. Li, G. Adili, G.-Y. Sun, M. Abuduaini, R. Abdulla, M. Maiwulanjiang, H.A. Aisa, Phenolic compounds and bioactivities from pomegranate (Punica granatum L.) peels, J. Agric. Food Chem. 70 (2022) 3678–3686, https://doi.org/10.1021/acs.jafc.1c08341.
[30] J.J. Sahayarayan, K.S. Rajan, R. Vidhyavathi, M. Nachiappan, D. Prabhu, S. Alfarraj, S. Arokiyaraj, A.N. Daniel, In-silico protein-ligand docking studies against the estrogen protein of breast cancer using pharmacophore based virtual screening approaches, Saudi J. Biol. Sci. 28 (2021) 400–407, https://doi.org/10.1016/j.sjbs.2020.10.023.
[31] C. Wang, W. Wu, A simple method to determine the R or S configuration of molecules with an axis of chirality, J. Chem. Educ. 88 (2011) 299–301, https://doi.org/10.1021/ed1003383.
[32] L. Barros, R.C. Calhelha, J.A. Vaz, I.C.F.R. Ferreira, P. Baptista, L.M. Estevinho, Antimicrobial activity and bioactive compounds of Portuguese wild edible mushrooms methanolic extracts, Eur. Food Res. Technol. 225 (2007) 151–156, https://doi.org/10.1007/s00217-006-0394-x.
[33] H. bouakline, I. Ziani, M.I. Yahyaoui, F. Corrias, A. Abdeslam, A. El Bachiri, Using green solvents as co-solvent in supercritical carbon dioxide extraction: A promising source of extracts rich in antioxidants and antimicrobials agents, Sustain. Chem. Pharm. 44 (2025) 101950, https://doi.org/10.1016/j.scp.2025.101950.
[34] M. Balouiri, M. Sadiki, S.K. Ibnsouda, Methods for in vitro evaluating antimicrobial activity: a review, J. Pharm. Anal. 6 (2016) 71–79, https://doi.org/10.1016/j.jpha.2015.11.005.
[35] Z. Peng, G. Wang, Q.H. Zeng, Y. Li, Y. Wu, H. Liu, J.J. Wang, Y. Zhao, Synthesis, antioxidant and anti-tyrosinase activity of 1,2,4-triazole hydrazones as antibrowning agents, Food Chem. 341 (2021) 128265, https://doi.org/10.1016/j.foodchem.2020.128265.
[36] Y. Zhang, R.A. Greer, Y. Song, H. Praveen, Y. Song, In silico identification of available drugs targeting cell surface BiP to disrupt SARS-CoV-2 binding and replication: drug repurposing approach, Eur. J. Pharm. Sci. 160 (2021) 105771, https://doi.org/10.1016/j.ejps.2021.105771.
[37] H. Sirous, G. Campiani, V. Calderone, S. Brogi, Discovery of novel hit compounds as potential HDAC1 inhibitors: The case of ligand-and structure-based virtual screening, Comput. Biol. Med. 137 (2021) 104808, https://doi.org/10.1016/j.compbiomed.2021.104808.
[38] J.W. Vant, S.-L.J. Lahey, K. Jana, M. Shekhar, D. Sarkar, B.H. Munk, U. Kleinekathöfer, S. Mittal, C. Rowley, A. Singharoy, Flexible fitting of small molecules into electron microscopy maps using molecular dynamics simulations with neural network potentials, J. Chem. Inf. Model 60 (2020) 2591–2604, https://doi.org/10.1021/acs.jcim.9b01167.
[39] M.H. Siddique, A. Ashraf, S. Hayat, B. Aslam, M. Fakhar-e-Alam, S. Muzammil, M. Atif, M. Shahid, S. Shafeeq, M. Afzal, Antidiabetic and antioxidant potentials of abelmoschus esculentus: in vitro combined with molecular docking approach, J. Saudi Chem. Soc. 26 (2022) 101418, https://doi.org/10.1016/j.jscs.2021.101418.
[40] V. de Almeida Paiva, I. de Souza Gomes, C.R. Monteiro, M.V. Mendonça, P. M. Martins, C.A. Santana, V. Gonçalves-Almeida, S.C. Izidoro, R.C. de Melo-Minardi, S. de Azevedo Silveira, Protein structural bioinformatics: an overview, Comput. Biol. Med. 147 (2022) 105695, https://doi.org/10.1016/j.compbiomed.2022.105695.
[41] N. Singh, L. Chaput, B.O. Villoutreix, Fast rescoring protocols to improve the performance of structure-based virtual screening performed on protein–protein interfaces, J. Chem. Inf. Model 60 (2020) 3910–3934, https://doi.org/10.1021/acs.jcim.0c00545.
[42] H. Bouammali, L. Zraibi, I. Ziani, M. Merzouki, L. Bourassi, E. Fraj, A. Challioui, K. Azzaoui, R. Sabbahi, B. Hammouti, Rosemary as a potential source of natural antioxidants and anticancer agents: a molecular docking study, Plants 13 (2023) 89, https://doi.org/10.3390/plants13010089.
[43] C.R. Baiz, B. Błasiak, J. Bredenbeck, M. Cho, J.-H. Choi, S.A. Corcelli, A.G. Dijkstra, C.-J. Feng, S. Garrett-Roe, N.-H. Ge, Vibrational spectroscopic map, vibrational spectroscopy, and intermolecular interaction, Chem. Rev. 120 (2020) 7152–7218, https://doi.org/10.1021/acs.chemrev.9b00813.
[44] L. Yang, Z. Sun, Y. Zu, C. Zhao, X. Sun, Z. Zhang, L. Zhang, Physicochemical properties and oral bioavailability of ursolic acid nanoparticles using supercritical anti-solvent (SAS) process, Food Chem. 132 (2012) 319–325, https://doi.org/10.1016/j.foodchem.2011.10.083.
[45] B. Kim, J.W. Han, M. Thi Ngo, Q. Le Dang, J.-C. Kim, H. Kim, G.J. Choi, Identification of novel compounds, oleanane-and ursane-type triterpene glycosides, from Trevesia palmata: their biocontrol activity against phytopathogenic fungi, Sci. Rep. 8 (2018) 14522, https://doi.org/10.1038/s41598-018-32956-4.
[46] A. Fălămaș, S.C. Pînzaru, C.A. Dehelean, C.I. Peev, C. Soica, Betulin and its natural resource as potential anticancer drug candidate seen by FT-Raman and FT-IR spectroscopy, J. Raman Spectrosc. 42 (2011) 97–107, https://doi.org/10.1002/jrs.2658.
[47] M.R. Dobbelaere, I. Lengyel, C.V. Stevens, K.M. Van Geem, Geometric deep learning for molecular property predictions with chemical accuracy across chemical space, J. Chemin.-. 16 (2024) 99, https://doi.org/10.1186/s13321-024-00895-0.
[48] H.I. Ansari, R.C. Dabhi, P.G. Trivedi, M.S. Thakar, J.J. Maru, G.M. Sindhav, Isolation and characterization of undescribed flavonoid from Abrus precatorius L. based on HPTLC-DPPH bioautography and its cytotoxicity evaluation, Futur. J. Pharm. Sci. 9 (2023) 119, https://doi.org/10.1186/s43094-023-00571-4.
[49] F.L.P. Costa, A.C.F. de Albuquerque, R.G. Fiorot, L.M. Lião, L.H. Martorano, G.V. S. Mota, A.L. Valverde, J.W.M. Carneiro, F.M. dos Santos Junior, Structural characterisation of natural products by means of quantum chemical calculations of NMR parameters: new insights, Org. Chem. Front 8 (2021) 2019–2058, https://doi.org/10.1039/D1QO00034A.
[50] J.A. De Jesus, M.D. Laurenti, L. Antonangelo, C.S. Faria, J.H.G. Lago, L.F. D. Passero, Related pentacyclic triterpenes have immunomodulatory activity in chronic experimental visceral leishmaniasis, J. Immunol. Res. 2021 (2021) 6671287, https://doi.org/10.1155/2021/6671287.
[51] G. Verardo, A. Gorassini, D. Fraternale, New triterpenic acids produced in callus culture from fruit pulp of Acca sellowiana (O. Berg) Burret, Food Res. Int. 119 (2019) 596–604, https://doi.org/10.1016/j.foodres.2018.10.037.
[52] A. Bruguière, S. Derbré, J. Dietsch, J. Leguy, V. Rahier, Q. Pottier, D. Bréard, S. Suor-Cherer, G. Viault, A.-M. Le Ray, MixONat, a software for the dereplication of mixtures based on ^{13}C NMR spectroscopy, Anal. Chem. 92 (2020) 8793–8801, https://doi.org/10.1021/acs.analchem.0c00193.
[53] Z.-W. Wu, W.-B. Li, J. Zhou, X. Liu, L. Wang, B. Chen, M.-K. Wang, L. Ji, W.-C. Hu, F. Li, Oleanane-and ursane-type triterpene saponins from Centella asiatica exhibit neuroprotective effects, J. Agric. Food Chem. 68 (2020) 6977–6986, https://doi.org/10.1021/acs.jafc.0c01476.
[54] M. Khin, S.L. Knowles, W.J. Crandall, D.D. Jones, Jr, N.H. Oberlies, N.B. Cech, J. Houriet, Capturing the antimicrobial profile of Rosmarinus officinalis against methicillin-resistant Staphylococcus aureus (MRSA) with bioassay-guided fractionation and bioinformatics, J. Pharm. Biomed. Anal. 197 (2021) 113965, https://doi.org/10.1016/j.jpba.2021.113965.
[55] S.A. Cinar, S. Ercan, S.E. Gunal, I. Dogan, V. Aviyente, The origin of exo-stereoselectivity of norbornene in hetero Diels–Alder reactions, Org. Biomol. Chem. 12 (2014) 8079–8086, https://doi.org/10.1039/C4OB01217H.
[56] S. Wang, D. Zhang, J. Zhu, H. Liu, B. Li, L. Huang, Achyrophenols A–F: polycyclic polyphenol lactone skeletons and a nor-ursane-type triterpenoid from achyrocline satureioides, J. Org. Chem. 86 (2021) 12813–12820, https://doi.org/10.1021/acs.joc.1c01447.
[57] M.A.M. Subbaiah, N.A. Meanwell, Bioisosteres of the phenyl ring: recent strategic applications in lead optimization and drug design, J. Med. Chem. 64 (2021) 14046–14128, https://doi.org/10.1021/acs.jmedchem.1c01215.
[58] Y. Li, J. Wang, L. Li, W. Song, M. Li, X. Hua, Y. Wang, J. Yuan, Z. Xue, Natural products of pentacyclic triterpenoids: From discovery to heterologous biosynthesis, Nat. Prod. Rep. 40 (2023) 1303–1353, https://doi.org/10.1039/D2NP00063F.
[59] L.N. Silva, K.R. Zimmer, A.J. Macedo, D.S. Trentin, Plant natural products targeting bacterial virulence factors, Chem. Rev. 116 (2016) 9162–9236, https://doi.org/10.1021/acs.chemrev.6b00184.
[60] L.P. Ferraz, T. da Cunha, A.C. da Silva, K.C. Kupper, Biocontrol ability and putative mode of action of yeasts against Geotrichum citri-aurantii in citrus fruit, Microbiol. Res 188–189 (2016) 72–79, https://doi.org/10.1016/j.micres.2016.04.012.
[61] H. Zhang, Y. Kang, N. Li, H. Wang, Y. Bao, Y. Li, X. Li, Z. Jiang, G. Chen, Triterpenoids from Liquidambar Fructus induced cell apoptosis via a PI3K-AKT related signal pathway in SMMC7721 cancer cells, Phytochemistry 171 (2020) 112228, https://doi.org/10.1016/j.phytochem.2019.112228.
[62] H. Zhang, L. Ma, M. Turner, H. Xu, X. Zheng, Y. Dong, S. Jiang, Salicylic acid enhances biocontrol efficacy of Rhodotorula glutinis against postharvest Rhizopus

rot of strawberries and the possible mechanisms involved, Food Chem. 122 (2010) 577–583, https://doi.org/10.1016/j.foodchem.2010.03.013.
[63] J.M. Andrade, E.M. Domínguez-Martín, M. Nicolai, C. Faustino, L.M. Rodrigues, P. Rijo, Screening the dermatological potential of plectranthus species components: antioxidant and inhibitory capacities over elastase, collagenase and tyrosinase, J. Enzym. Inhib. Med. Chem. 36 (2021) 257–269, https://doi.org/10.1080/14756366.2020.1862099.
[64] Z. Ozdemir, D. Saman, L. Bednarova, M. Pazderkova, L. Janovska, Nonappa, Z. Wimmer, Aging-induced structural transition of nanoscale oleanolic acid amphiphiles and selectivity against gram-positive bacteria, ACS Appl. Nano Mater. 5 (2022) 3799–3810, https://doi.org/10.1021/acsanm.1c04374.
[65] S. Baghel, H. Cathcart, N.J. O'Reilly, polymeric amorphous solid dispersions: a review of amorphization, crystallization, stabilization, solid-state characterization, and aqueous solubilization of biopharmaceutical classification system class II drugs, J. Pharm. Sci. 105 (2016) 2527–2544, https://doi.org/10.1016/j.xphs.2015.10.008.
[66] S.R. Byrn, R.R. Pfeiffer, G. Stephenson, D.J.W. Grant, W.B. Gleason, Solid-state pharmaceutical chemistry solid-state pharmaceutical chemistry, Chem. Mater. 6 (1994) 1148–1158, https://doi.org/10.1021/cm00044a013.
[67] R. Biswas, J. Chanda, A. Kar, P.K. Mukherjee, Tyrosinase inhibitory mechanism of betulinic acid from Dillenia indica, Food Chem. 232 (2017) 689–696, https://doi.org/10.1016/j.foodchem.2017.04.008.
[68] M.M. Rahman, P.S. Dhar, F. Anika, L. Ahmed, M.R. Islam, N.A. Sultana, S. Cavalu, O. Pop, A. Rauf, Exploring the plant-derived bioactive substances as antidiabetic agent: an extensive review, Biomed. Pharm. 152 (2022) 113217, https://doi.org/10.1016/j.biopha.2022.113217.
[69] S.-C. Liu, M.-L. Sheu, Y.-C. Tsai, Y.-C. Lin, C.-W. Chang, D.-W. Lai, Attenuation of in vitro and in vivo melanin synthesis using a Chinese herbal medicine through the inhibition of tyrosinase activity, Phytomedicine 95 (2022) 153876, https://doi.org/10.1016/j.phymed.2021.153876.
[70] H. Kieserling, W.J.C. de Bruijn, J. Keppler, J. Yang, S.T. Sagu, D. Güterbock, H. Rawel, K. Schwarz, J. Vincken, A. Schieber, Protein–phenolic interactions and reactions: discrepancies, challenges, and opportunities, Compr. Rev. Food Sci. Food Saf. 23 (2024) e70015, https://doi.org/10.1111/1541-4337.70015.
[71] K. Khezri, M. Saeedi, K. Morteza-Semnani, J. Akbari, S.S. Rostamkalaei, An emerging technology in lipid research for targeting hydrophilic drugs to the skin in the treatment of hyperpigmentation disorders: kojic acid-solid lipid nanoparticles, Artif. Cells, Nanomed., Biotechnol. 48 (2020) 841–853, https://doi.org/10.1080/21691401.2020.1770271.
[72] R. Kumari, S. Kumar, In silico characterization, homology modeling and virtual screening of selected natural compounds as modulators of salmo salar and teratodon nigrovirdis tyrosinase protein, Int. J. Curr. Microbiol. Appl. Sci. 9 (2020) 1172–1181, https://doi.org/10.20546/ijcmas.2020.903.137.
[73] J.L. Shamshina, R.D. Rogers, Ionic liquids: new forms of active pharmaceutical ingredients with unique, tunable properties, Chem. Rev. 123 (2023) 11894–11953, https://doi.org/10.1021/acs.chemrev.3c00384.
[74] W. Teng, Z. Zhou, J. Cao, Q. Guo, Recent Advances of Natural Pentacyclic Triterpenoids as Bioactive Delivery System for Synergetic Biological Applications, Foods 13 (2024) 2226, https://doi.org/10.3390/foods13142226.
[75] W. Gao, B. Mu, F. Yang, Y. Li, X. Wang, A. Wang, Multifunctional honeysuckle extract/attapulgite/chitosan composite films containing natural carbon dots for intelligent food packaging, Int. J. Biol. Macromol. 280 (2024) 136042, https://doi.org/10.1016/j.ijbiomac.2024.136042.
[76] G.E.-S. Batiha, D.E. Hussein, A.M. Algammal, T.T. George, P. Jeandet, A.E. Al-Snafi, A. Tiwari, J.P. Pagnossa, C.M. Lima, N.D. Thorat, application of natural antimicrobials in food preservation: Recent views, Food Control 126 (2021) 108066, https://doi.org/10.1016/j.foodcont.2021.108066.
[77] S. Arokiyaraj, Y. Dinakarkumar, H. Shin, A comprehensive overview on the preservation techniques and packaging of processed meat products: emphasis on natural derivatives, J. King Saud. Univ. 36 (2023) 103032, https://doi.org/10.1016/j.jksus.2023.103032.
[78] B.G. Bag, R. Majumdar, Self-assembly of renewable nano-sized triterpenoids, Chem. Rec. 17 (2017) 841–873, https://doi.org/10.1002/tcr.201600123.
[79] N.A. Bahmid, S.A. Siddiqui, Factors influencing release, absorption, and concentration of natural compounds in antimicrobial packaging, Food Rev. Int. 40 (2024) 1554–1580, https://doi.org/10.1080/87559129.2023.2224439.
[80] R. Priyadarshi, J.-W. Rhim, Chitosan-based biodegradable functional films for food packaging applications, Innov. Food Sci. Emerg. Technol. 62 (2020) 102346, https://doi.org/10.1016/j.ifset.2020.102346.
[81] M. Asgher, S.A. Qamar, M. Bilal, H.M.N. Iqbal, Bio-based active food packaging materials: Sustainable alternative to conventional petrochemical-based packaging materials, Food Res. Int. 137 (2020) 109625, https://doi.org/10.1016/j.foodres.2020.109625.
[82] O. Fedotova, D. Myalenko, N. Pryanichnikova, E. Yurova, E. Agarkova, Microscopic and structural studies of an antimicrobial polymer film modified with a natural filler based on triterpenoids, Polym. (Basel) 14 (2022) 1097, https://doi.org/10.3390/polym14061097.
[83] C. Castiello, P. Junghanns, A. Mergel, C. Jacob, C. Ducho, S. Valente, D. Rotili, R. Fioravanti, C. Zwergel, A. Mai, GreenMedChem: the challenge in the next decade toward eco-friendly compounds and processes in drug design, Green. Chem. 25 (2023) 2109–2169, https://doi.org/10.1039/D2GC03772F.
[84] E. Maurizzi, F. Bigi, A. Quartieri, R. De Leo, L.A. Volpelli, A. Pulvirenti, The green era of food packaging: general considerations and new trends, Polym. (Basel) 14 (2022) 4257, https://doi.org/10.3390/polym14204257.